

## The Lupus clouds

Fernando Comerón

*European Southern Observatory*  
*Karl-Schwarzschild-Str. 2*  
*D-85737 Garching bei München*  
*Germany*

**Abstract.** The Lupus clouds compose one of the main low-mass star forming complexes within 200 pc of the Sun. They contain four main star forming sites, including the rich T Tauri association in Lupus 3. They are located in the Scorpius-Centaurus OB association, whose massive stars are likely to have played a significant role in the evolution and perhaps the origin of the complex. The entire variety of objects related to the various stages of early stellar evolution are represented in Lupus, including some of the best studied T Tauri stars like RU Lup. The determination of many properties of the clouds, as well as their associated stellar population, are limited by the uncertainty with which the distance is known. We argue that a single value of the distance is probably inadequate to be representative of the entire complex, and that depth effects are likely to be significant, as expected from its large extent on the plane of the sky. The total mass of molecular gas in the complex is a few times  $10^4 M_{\odot}$ . The most distinctive property of its stellar population is the outstanding abundance of mid M-type pre-main sequence stars. Some likely substellar objects have been identified as well, particularly thanks to mid-infrared observations carried out with the Spitzer Space Observatory. A widely distributed young low-mass population of weak-line T Tauri stars, identified by its X-ray emission, is observed in the direction of Lupus but it is probably related to the Gould Belt rather than to the star forming complex. A few individual objects of particular interest are briefly reviewed: the Herbig Ae/Be stars HR 5999 and HR 6000 that dominate the Lupus 3 cloud, the classical T Tauri star RU Lup, the EXor class prototype EX Lup, the very low luminosity, outflow-driving sources HH 55 and Par-Lup3-4, the extreme emission-line star Th 28, and the binary object GQ Lup composed of an ordinary T Tauri star with a substellar companion of possible planetary mass.

### 1. Introduction

The *Lupus clouds* is the generic denomination of a loosely connected concentration of dark clouds and low-mass pre-main sequence stars lying in the direction of that constellation, between Galactic longitudes  $334^{\circ} < l < 352^{\circ}$  and latitudes  $+5^{\circ} < b < +25^{\circ}$ . In terms of angular extent it is one of the largest low-mass star forming complexes on the sky, and it also contains one of the richest associations of T Tauri stars. Its distance places it among the nearest star forming regions, together with those in Corona Australis, Ophiuchus, Taurus-Auriga, and Chamaeleon, all of which are described elsewhere in this volume. In size and contents the Lupus clouds are comparable to those other complexes.

The earliest description of the Lupus dark clouds in the literature is probably the one given by E.E. Barnard in his *Catalogue of Dark Objects in the Sky* (Barnard 1927). One of the most prominent clouds of the Lupus complex, entry number 228 in Barnard's

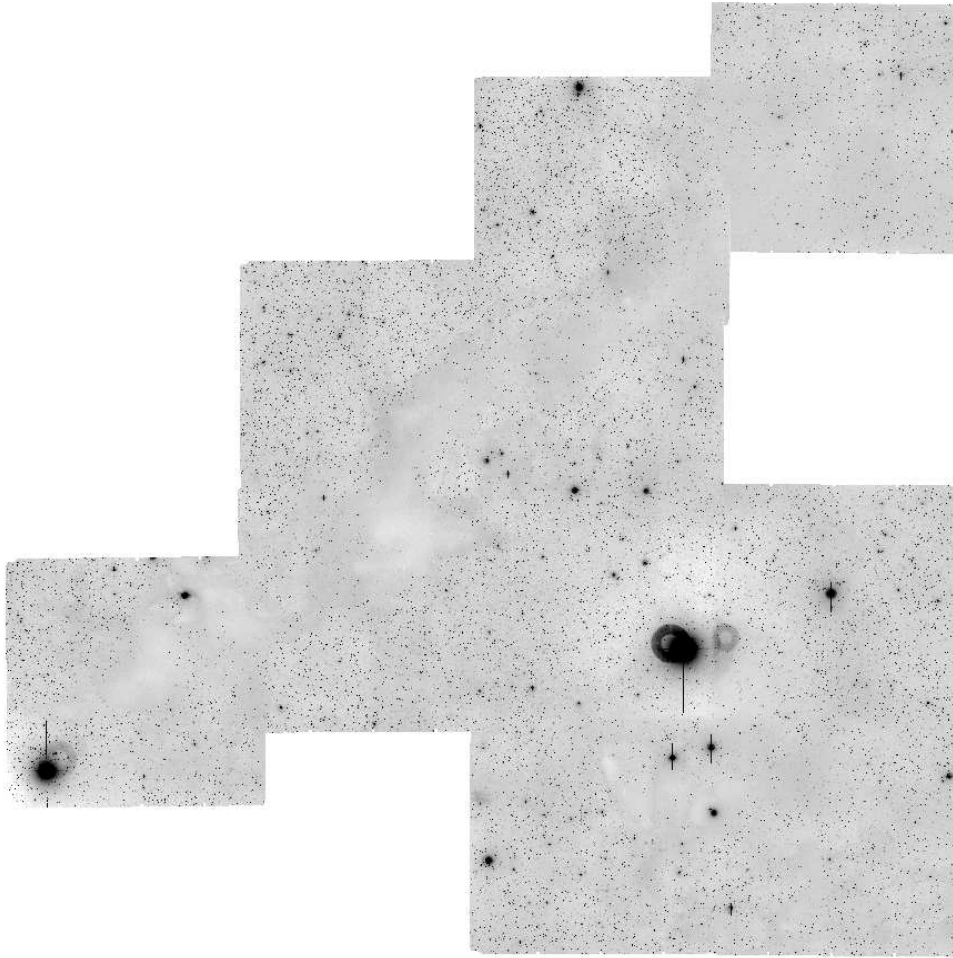


Figure 1. A large-area mosaic of the Lupus 1 cloud composed of images taken through the  $R$  filter using the Wide Field Imager on the MPI-ESO 2.2m telescope on La Silla. The field measures  $129' \times 129'$  and is centered at  $\alpha(2000) = 15 : 42 : 00$ ,  $\delta(2000) = -34 : 03$ . North is at the top and East to the left. The field covered includes the thickest parts of the dark nebulosity in the region, and may be compared to Figure 9. From a still unpublished survey by the author in support of the Spitzer ‘Cores to Disks’ Legacy program.

catalog, is described as a *Large vacant region about 4 degrees long NW and SE. This vacant region is about 4 degrees long, extending from RA=15h31m, dec=-32°45' to RA=15h43m, dec=-35°30' [1875 equinox]. Its average width is about 1/2 degree. It is strongest marked at the north end. There are fragments of other dark markings several degrees west of this.* Barnard’s cloud, B228 (Figure 1), is more frequently referred to as Lupus 1 in modern literature, following the denominations originally proposed by Thé (1962), and is one of the major dark clouds in the region (see Section 4.). Molecular-line surveys, initiated with the  $^{12}\text{CO}(J 1 \rightarrow 0)$  observations of Murphy et al. (1986) and large-scale extinction maps of the region have revealed additional

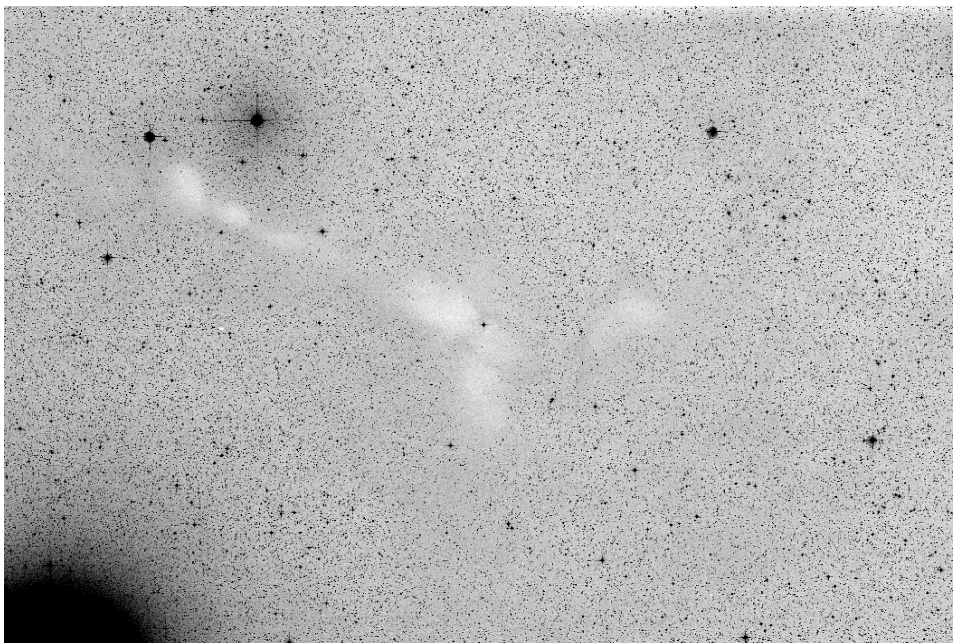


Figure 2. Image of the Lupus 2 cloud in the Digitized Sky Survey. The field is centered on the T Tauri star RU Lup and it measures  $90' \times 60'$ . North is at the top and East to the left. The bright star at the bottom left corner is  $\eta$  Lup.

concentrations that add up to a total mass of molecular gas estimated at  $\sim 4 \times 10^4 M_{\odot}$  distributed in several major concentrations (Figures 2, 3, 4).

The association of young stellar objects with the Lupus clouds was recognized very early. Lupus 2 contains one of the most active T Tauri stars known, RU Lup (see Sect. 7.2.), whose peculiar spectrum was first described in some detail by Merrill (1941). Shortly afterwards it was included as one of the eleven initially proposed members defining the T Tauri class in the milestone paper of Joy (1945), where the frequent association of such stars with dark clouds was already noted. The nature of the Lupus clouds as a recent star forming site was thus implicitly recognized later by the works of Herbig (1952) and Walker (1956) where the pre-main sequence character and very young age of T Tauri stars was identified.

The first aggregate of T Tauri stars in Lupus was discovered in the Lupus 1 cloud by Henize (1954), who remarked on its similarity with the R CrA association. A much more spatially extended population of 39 T Tauri stars was found by Thé (1962), who pointed out their concentration into three spatially distinct groups, named as Lupus 1, 2, and 3 (Figure 9). The distinction into those three groups (which recent molecular-line surveys have shown *not* to coincide with the largest concentrations of molecular gas in the complex) is widely in use today. The census of known T Tauri members in Lupus was nearly duplicated by Schwartz (1977) in his search for Southern Herbig-Haro objects and emission-line stars, who listed 69 such objects in the region, some of them in an additional group labeled as Lupus 4 in that work. The vast majority of such stars have been confirmed as members with further spectroscopy. Virtually the entire content of classical T Tauri stars known nowadays in the Lupus clouds is included in Schwartz's catalog, but the stellar census of three of the clouds, Lupus 1, 3,

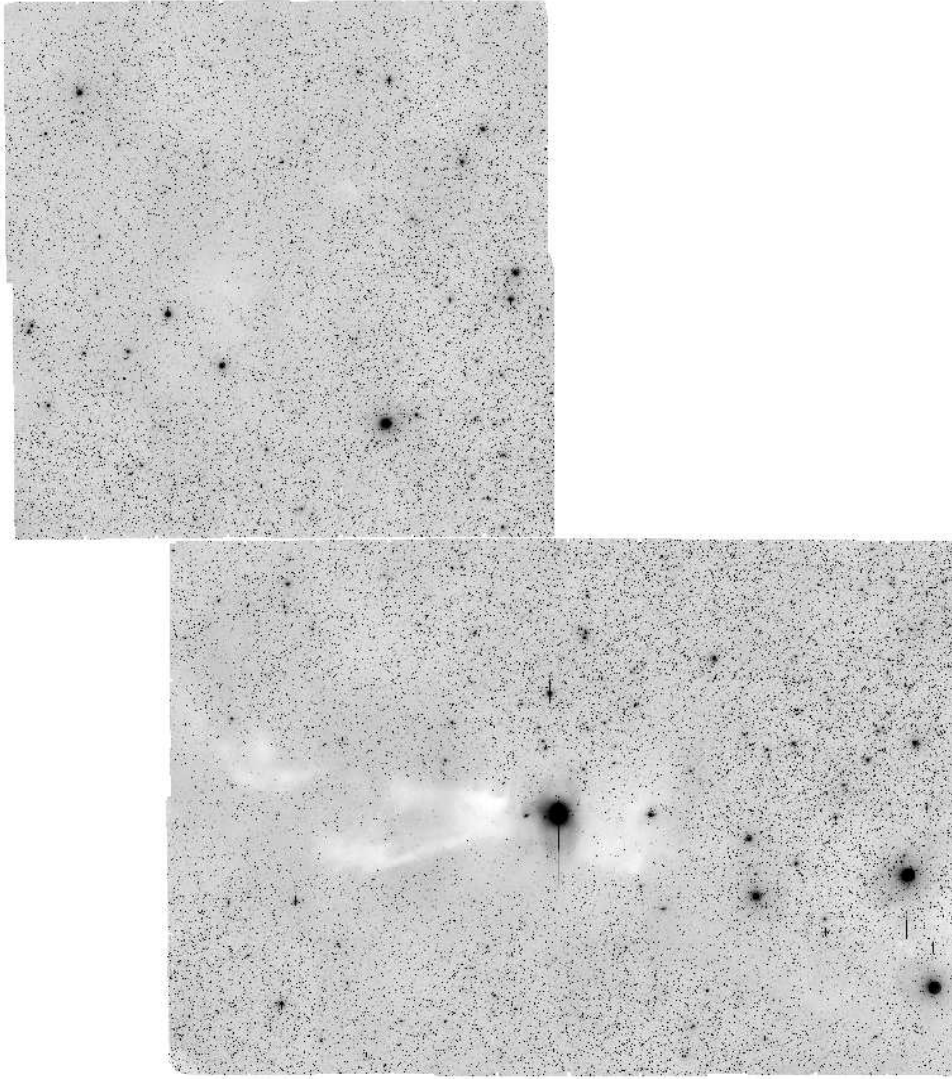


Figure 3. A large-area mosaic of the Lupus 3 cloud composed of images taken through the  $R$  filter using the Wide Field Imager on the MPI-ESO 2.2m telescope on La Silla. The field measures  $112' \times 126'$  and is centered at  $\alpha(2000) = 16 : 09 : 20$ ,  $\delta(2000) = -38 : 33$ . North is at the top and East to the left. The bottom part of the field covers the thick clouds containing HR 5999 and HR 6000 (the bright stars near the center of the bottom half of the field), clearly delineated against the backdrop of background stars. The Northeastern half of the field corresponds to less dense clouds also part of Lupus 3. A comparison with Figure 9 shows the location of the field, on the Eastern side of the area assigned to Lupus 3 in Figure 9. From a still unpublished survey by the author in support of the Spitzer ‘Cores to Disks’ Legacy program.

and 4, has been greatly expanded with the identification of new low-mass and even substellar members by the recent infrared observations carried out with the Spitzer Space Observatory (Merín et al. 2008). The stellar population of the Lupus clouds is composed of low-mass stars, with the only exception of two intermediate-mass Herbig

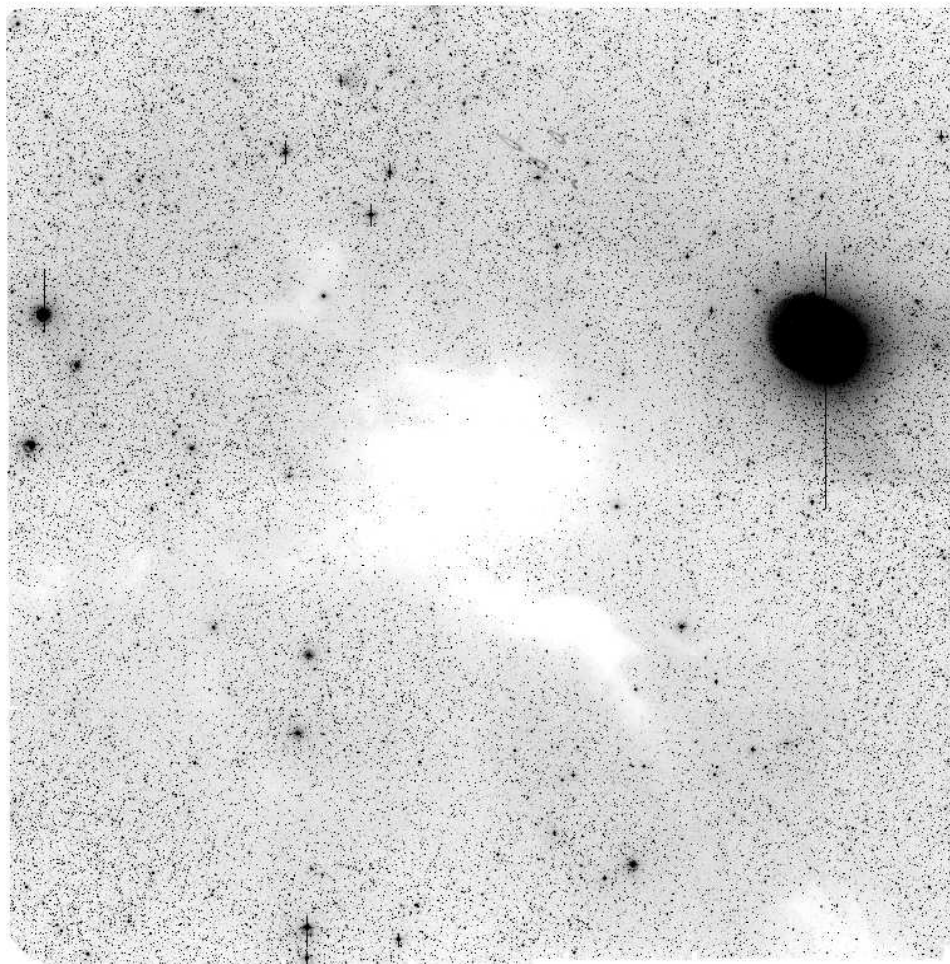


Figure 4. A large-area mosaic of the Lupus 4 cloud composed of images taken through the  $R$  filter using the Wide Field Imager on the MPI-ESO 2.2m telescope on La Silla. The field measures  $62' \times 64'$  and is centered at  $\alpha(2000) = 16 : 01 : 32$ ,  $\delta(2000) = -41 : 54$ . North is at the top and East to the left. The densest dark cloud in Lupus 4 appears at the center of the image, standing out against the rich background stellar field at its relatively low Galactic latitude. Its extension to the Southwest, also visible in Figure 9, can be easily traced. From a still unpublished survey by the author in support of the Spitzer ‘Cores to Disks’ Legacy program.

Ae/Be stars, HR 5999 and HR 6000 in the Lupus 3 cloud (see Section 6.). The overall star-forming history and distribution in the region has proven to be more complicated than previously thought after the discovery by the ROSAT X-ray satellite of an extended population of weak-line T Tauri stars, first identified by their X-ray emission (Krautter et al. 1997; see also Section 6.), which greatly exceeds in number the classical T Tauri star population coincident with the clouds.

Further studies have used different techniques to increase the stellar and substellar census of the Lupus clouds (e.g. Nakajima et al. 2000, Comerón et al. 2003, López Martí et al. 2005). At the same time, new observations that we review in the coming

Sections have provided detailed views on the distribution and physical properties of the interstellar gas (e.g. Tachihara et al. 1996, 2001, Hara et al. 1999).

Given the extensive review of the work on the Lupus clouds until the late 1980s presented by Krautter (1991), we focus here on advancements of our knowledge of the region that have taken place in the last decade and a half. Some of the most outstanding contributions have been very recently provided by the sensitive infrared observations carried out by the Spitzer Space Telescope, particularly in the framework of the Spitzer Legacy Program "From cores to disks" (Evans et al. 2003). We include in this review a selection of early results obtained by this program on the Lupus region.

## 2. Relationship to Larger Structures

The Lupus clouds are projected on the sky against the nearest and one of the best studied OB associations, Scorpius-Centaurus (e.g. Blaauw 1991, de Geus et al. 1989, de Geus 1992, Preibisch et al. 2002; see also chapter by Preibisch & Mamajek). The Scorpius-Centaurus association is a vast complex including over 300 astrometrically confirmed early-type members (de Zeeuw et al. 1999) and spans nearly  $90^\circ$  in Galactic longitude, at an average distance of  $\sim 140$  pc from the Sun. Most of the Scorpius-Centaurus association is well detached from the Galactic disk and its members are found at Galactic latitudes of up to  $+32^\circ$ . Scorpius-Centaurus, together with Perseus OB2 and the Orion complex, is one of the main structures of the *Gould Belt* (Pöppel 1997), the extended disk-like arrangement of OB associations, molecular clouds and other tracers of recent star formation that dominates the solar neighborhood up to a distance of  $\sim 600$  pc. The tilt of  $20^\circ$  degrees of the midplane of the Gould Belt with respect to the Galactic equator (Comerón et al. 1994) facilitates the recognition of its member structures, especially near the direction of its apsis which lies towards  $l \simeq 10^\circ$ , not far from the location of the Lupus clouds. The high Galactic latitude at which the bulk of the Lupus complex is seen greatly reduces the likelihood of chance alignments with background, unrelated star forming regions.

The estimated distance of 140-200 pc to the Lupus clouds (see Sect. 3.) matches well the distance to the Scorpius-Centaurus association, leaving little doubt as to the physical relationship between both entities. The existence of several distinct, spatially separated groups is well established in Scorpius-Centaurus, as well as differences among the average ages of the stars of each group. The Lupus clouds occupy a gap between two such groups, namely Upper Scorpius (age 5-6 Myr; de Geus et al. 1989, Preibisch et al. 2002) and Upper Centaurus-Lupus (age 14 Myr; de Geus et al. 1989); see Figure 5 and probably represents a more recent episode of star formation in the region. The region of the sky occupied by the Lupus clouds is devoid of the early-type stars that are found in both groups, and there is no current indication in the Lupus clouds of any ongoing high-mass star forming activity (see Sect. 6.). However, the abundant presence of OB members of Scorpius-Centaurus in the vicinity of the Lupus complex implies the existence of an ambient field of ultraviolet radiation much more intense than that in which other isolated star forming regions are immersed, which probably has noticeable effects on the physical conditions of its associated interstellar medium (see Sect. 4.). Such high-energy radiation adds to the mechanical energy injected into the Lupus clouds by stellar winds of the nearby OB stars and by the explosion as supernovae of ancient members of the OB association. These sources of energy are likely to have played an important role in the evolution and possibly the origin of the Lupus

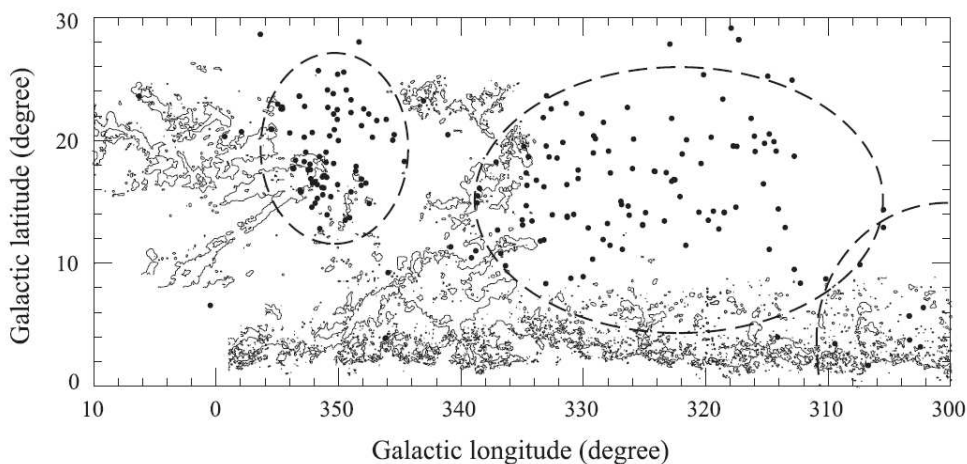


Figure 5. Location of the Lupus clouds in the Scorpius-Centaurus association. The thin contours outline the distribution of molecular gas traced by CO in the region. The dots correspond to OB stars. The dashed lines mark the approximate contours of the Scorpius-Centaurus subgroups defined by Blaauw (see Blaauw 1991). The Lupus clouds are the structure extending toward high latitudes left of the center, between  $334^\circ$  and  $352^\circ$ . The clouds also at high latitude near the left edge of the figure belong to the Ophiuchus complex. From Tachihara et al. (2001).

complex (Tachihara et al. 2001). It should be noted that the Ophiuchus complex, which lies at a similar distance from the Sun and has a similar mass of molecular gas but more vigorous star forming activity (see review by Wilking et al. in this volume) occupies a position with respect to Lupus that is roughly symmetric with respect to the center of the Upper Scorpius OB group.

The scenario of a common origin of both the Ophiuchus and Lupus complexes has been considered by some authors (e.g. Tachihara et al. 2001 and references therein). The possibility and indirect evidence of a violent origin of Ophiuchus have been explored by Preibisch & Zinnecker (1999), who proposed a supernova explosion in the Upper Scorpius group about 1.5 Myr ago. This is the estimated age of an expanding shell centered in Upper Scorpius, detected in HI maps, and currently engulfing both complexes (de Geus 1992), which lends plausibility to such scenario. The overall distribution of  $^{12}\text{CO}$  emission in the Lupus complex is roughly arc-like and is located near the rim of the HI shell, which suggests that the explosive event that may have triggered star formation in the Ophiuchus clouds may also be responsible for the morphology and star forming activity in Lupus. Both Ophiuchus and Lupus are thus located in an environment disturbed by the existence of nearby hot stars and their large-scale dynamical effects on their surrounding interstellar medium. This makes them interesting targets for comparative studies with respect to other nearby regions having similar molecular masses and low-mass star formation activity, such as the Taurus-Auriga and the Chamaeleon clouds (see chapters by Kenyon et al. and Luhman, respectively, elsewhere in this volume), but having evolved in isolation and relatively unperturbed.

The possible relationship of structures seen in maps of extended high-energy emission in the direction of Lupus with the molecular clouds is intriguing. The so-called *Lupus Void* is a soft X-ray-emitting region (=H1538-32; Riegler et al. 1980) some  $3^\circ \times 4^\circ$  across, apparently devoid of dust and thus appearing as a region of low far-infrared

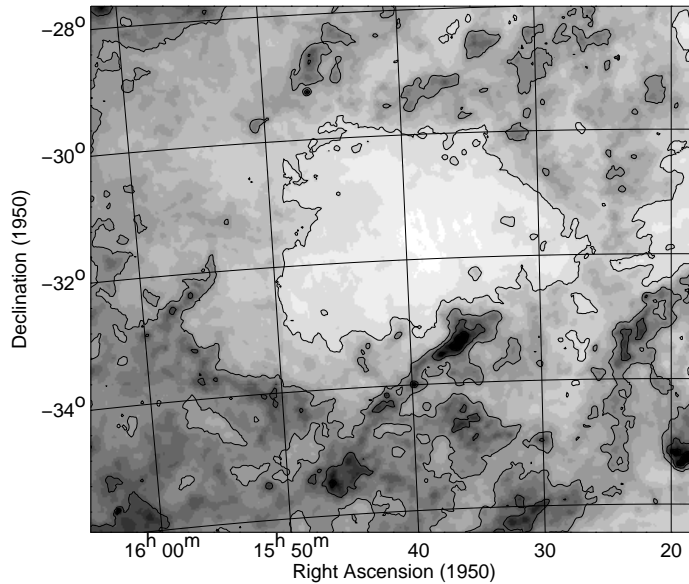


Figure 6. A  $100\ \mu\text{m}$  IRAS map of the Lupus void, which appears as the lighter area near the center of the image. The darkest shades of grey below the void are caused by dust emission in the Lupus 1 cloud. From Franco (2002).

emission, as shown in Figure 6. The correspondence of the void with a region of decreased  $100\ \mu\text{m}$  emission was noted by Gahm et al. (1990), who supported its interpretation as a young supernova remnant as already proposed by Riegler et al. (1980). Recent studies of the stellar population seen in its direction have led Franco (2002) to suggest that the Lupus Void is actually unrelated to the Lupus clouds, and a structure whose near edge lies in front of Scorpius-Centaurus at a distance of only 60 to 100 pc. Using linear polarization measurements, Alves & Franco (2006) find low levels of polarization on stars up to 250 pc in directions not intercepted by Lupus 1, suggesting that a large region around the cloud is cleared off from dust. According to Franco (2002), rather than a real entity the Lupus Void seems to be an enhancement in soft X-ray emission due to the lower density of absorbing dust in the interface between the *Lupus Loop*, which is an old supernova remnant (e.g. Leahy et al. 1991), and the Local Bubble (e.g. Cox & Reynolds 1987; Franco 1990; Fuchs et al. 2006) in which the Sun is immersed. CO observations also confirm that the Lupus Void is devoid of molecular gas (Tachihara et al. 2001). The clearing off of dust may be the result of hydromagnetic instabilities in the interface between both bubbles (Breitschwerdt et al. 2000).

### 3. Distance

While the Lupus clouds have been always recognized as one of the nearest star forming regions (see Gahm et al. 1993 for references to early distance determinations), their precise distance is still a matter of debate, with recent derivations suggesting values that range from 100 pc to over 300 pc for at least parts of the complex. Most of the distance

determinations agree on a smaller range, between 140 pc and 240 pc. Such a range is still uncomfortably large, as it implies an uncertainty by a factor near 3 in important quantities that depend on the square of the distance, such as the mass of clouds and cores or the luminosity of its member stars. Some of the most highly discrepant values refer to specific clouds, suggesting that some parts of the complex might be unrelated to the rest (Knude & Nielsen 2001). However, the narrow range of mean velocities within which the entire region is contained ( $\simeq 3 \text{ km s}^{-1}$  among the mean velocities of the different clouds; e.g. Tachihara et al. 1996, Vilas-Boas et al. 2000) argues in favor of the coherence of the whole complex as a single structure.

The *average* distances to the subgroups of the Scorpius-Centaurus association have been well established thanks to the numerous stars in the region whose trigonometric parallaxes have been measured by the Hipparcos astrometric satellite. Based on Hipparcos measurements, de Zeeuw et al. (1999) find a distance of  $145 \pm 2$  pc for Upper Scorpius, and  $140 \pm 2$  pc for Upper Centaurus-Lupus, the two groups adjacent to the Lupus clouds. However, assuming that both groups are roughly spherical their considerable extent on the sky ( $\sim 25^\circ$  for Upper Centaurus-Lupus,  $\sim 14^\circ$  for Upper Scorpius) implies a significant depth, yielding a diameter of  $\sim 60$  pc for Upper Centaurus-Lupus and  $\sim 35$  pc for Upper Scorpius, thus preventing us from directly adopting the average distances to both groups as the precise distance to the Lupus clouds. The same caveat is of course valid for the Lupus clouds themselves, which span over an arc of  $\sim 20^\circ$  of the sky, corresponding to nearly 50 pc at the distance of Scorpius-Centaurus and thus to a similar depth if the angular extent is comparable to the extent along the line of sight.

In their pioneering work on the molecular gas in the region, Murphy et al. (1986) suggested the possibility that the gap in the distribution of early-type stars between both Scorpius-Centaurus groups may be due to obscuration by the Lupus complex, which would thus be located in the foreground. The idea has been ruled out by further surveys of the region (Preibisch et al. 2002), which show the gap to be real and the two groups to be physically separated, thus leaving unconstrained the relative location of the OB groups and the complex.

Most distance determinations to the Lupus clouds found in the literature rely on the combined use of approximate distances to individual stars and estimates of their reddening. Due to their pre-main sequence status, spectroscopic distance estimates to the members of the clouds themselves are not possible without previous knowledge of the ages. For this reason, determinations of distances to the clouds using these methods have relied upon non-member main sequence stars with known intrinsic colors seen towards the same general direction, for which the distance may be derived to a sufficient accuracy from the spectral type and the photometry. The distance of the clouds is then found by examining the distribution of reddening towards stars at different distances, and identifying the distance at which the reddening shows a jump due to the dust associated with the clouds. Such a method was used by Franco (1990), who derived a distance of  $165 \pm 15$  pc based on the distribution of reddening in Kapteyn's Selected Area 179, located near the Lupus 4 cloud. Further studies by Franco (2002) using Strömgren photometry of stars near Lupus 1 in the region of the Lupus Void (see Section 2.) and by Alves & Franco (2006) using linear polarization towards stars with known distances in the same region confirm an extinction and polarization jump at 130-150 pc. Such results are consistent with those obtained by Hughes et al. (1993) who used photometry and spectroscopy of field stars, particularly F and G types, to derive distances and extinctions. The distance of  $140 \pm 20$  pc to the Lupus complex that they

find has been commonly adopted in many further studies. An important improvement in this technique, relying both on a greater number of probe stars and on a robust statistical analysis, has been recently presented by Lombardi et al. (2008), who obtain a distance of  $155 \pm 8$  pc but with hints of significant depth effects, which we discuss below.

A general agreement is found in the pre-Hipparcos literature among the different distance determinations using variations of the method described above, which tend to yield results in the 130-170 pc range. It may thus seem somewhat surprising that new derivations carried out based on the trigonometric distances directly derived from Hipparcos data yield larger scatter and some puzzling discrepancies. Using extinctions and Hipparcos trigonometric parallaxes of field stars observed in the direction of several nearby star forming clouds, Knude & Høg (1998) estimated a distance of only 100 pc for the Lupus complex. On the other end of the range, Knude & Nielsen (2001) suggested a distance of 360 pc to the Lupus 2 cloud based on Hipparcos parallaxes and  $V - I$  colors. Such a distance, placing it over twice as far away as the other clouds, would imply that Lupus 2 is an unrelated background cloud projected by chance on the same position of the sky as the rest of the complex. The parallax measured by Hipparcos for the main stellar member of Lupus 2, RU Lup (Sect. 7.2., is  $4.34 \pm 3.56$  mas, which hints at a much closer distance. Nevertheless, the relatively large uncertainty of the parallax obtained by Hipparcos for RU Lup is of little help in constraining the distance to its host cloud.

A more detailed approach to the extinction jump method has been adopted by Crawford (2000), who obtained medium-to-high resolution spectroscopy in the region of the interstellar NaI D lines of 29 B and A stars in Scorpius-Centaurus near Lupus, with parallaxes measured by Hipparcos. The depth of the NaI absorption thus replaces the extinction as a probe of the intervening gas, providing in addition information on the kinematics of the absorbing medium and on the possible existence of kinematically different components. The distance to the Lupus complex obtained by Crawford (2000),  $150 \pm 10$  pc, is in good agreement with other determinations but in conflict with the one of Knude & Høg (1998) cited above. Crawford identifies the likely source of discrepancy with that work as due to an additional, foreground absorbing layer related to the expanding shell around Upper Scorpius, which is detected in the spectra of the nearest stars in the sample as a blueshifted component. The effects of this layer are also detected in polarization measurements of stars towards the Lupus Void by Alves & Franco (2006), and estimated to lie at 60-100 pc. In turn, the absorption actually associated with the Lupus clouds is clearly identified as having a positive velocity of a few  $\text{km s}^{-1}$ .

The availability of the Hipparcos data also allows in principle the use of directly measured trigonometric parallaxes of members of star forming clouds. Given the relatively bright limiting magnitude reached by Hipparcos, high precision parallaxes are available only for the brightest members of each star forming region. Results on such measurements have been presented by Wichmann et al. (1998) and Bertout et al. (1999) for several nearby star forming regions and, in Bertout et al.'s work, also for isolated pre-main sequence stars. Five members of the Lupus clouds, including the already mentioned RU Lup, are included by both studies in the analysis. A sixth member, the close binary IM Lup, is excluded from both studies due to its meaningless astrometric solution. The individual parallaxes of these stars are listed in Table 1. An additional parallax determination has been recently presented by Neuhauser et al. (2008) for the

Table 1. Hipparcos parallaxes of Lupus members

| Star    | Cloud | parallax (mas)    | distance (pc)        | Notes |
|---------|-------|-------------------|----------------------|-------|
| IM Lup  | 2     | $-4.77 \pm 13.79$ | -                    | 1, 2  |
| RU Lup  | 2     | $4.34 \pm 3.56$   | $230^{+1050}_{-103}$ | 2     |
| RY Lup  | 4     | $9.26 \pm 2.83$   | $108^{+48}_{-25}$    | 2     |
| Sz 68   | 1     | $6.29 \pm 2.05$   | $159^{+77}_{-39}$    | 2     |
| HR 5999 | 3     | $4.81 \pm 0.87$   | $208^{+46}_{-32}$    | 3     |
| HR 6000 | 3     | $4.15 \pm 0.83$   | $241^{+60}_{-40}$    | 4     |

Notes:

1: poor astrometric solution; resolved binary

2: Classical T Tauri star

3: Herbig Ae star

4: B peculiar star

GQ Lup system (see Section 7.7.), which yields a distance of  $156 \pm 50$  pc for the primary.

Formally, the conclusion of both works is that the distance to the complex appears to be larger than previous estimates. As Bertout et al. (1999) point out and can be easily seen in Table 1, this conclusion largely rests on the parallaxes of the HR 5999/6000 pair, which are the stars having the most accurate measurements. A shorter distance, in better agreement with other determinations, is suggested by RY Lup, and perhaps also by Sz 68.

In view of the significant depth effects that may be expected among the clouds composing the Lupus complex as noted above it is important to consider the details of the different distance determinations quoted above, and particularly the locations of the stars upon which they rest. We first note that the stars associated with Lupus 1 and 2 (only one for each cloud) have a large uncertainty in their measured parallax, making the latter compatible with any of the other measurements. On the other hand, the best constraints on the distance measured by Hughes et al. (1993),  $140 \pm 20$  pc, come from stars seen towards Lupus 1 and is consistent with the robust lower limit found by Crawford (2000) towards the same cloud. Also the distance determined by Franco (2002) largely refers to Lupus 1. The previous determination by the same author cited above (Franco 1990),  $165 \pm 15$  pc, is based on a field near Lupus 4 and is marginally consistent with the distance to RY Lup. Similar caveats apply to the thorough determination by Lombardi et al. (2008), which is dominated by the stars located at lower Galactic latitudes, mainly Lupus 4 and 6. Unfortunately, both Lupus 1 and 3 are probed by a small number of stars (6 and 3, respectively) and no suitable star is placed as a possible probe of Lupus 2. The distance to the higher latitude clouds of the Lupus region remains thus undetermined by this new analysis.

Given the locations of the stars that have been used in the different distance determinations, it seems reasonable to interpret the differences among them as providing evidence for the depth of the complex along the line of sight, rather than as implying a conflict between the Hipparcos measurements and previous determinations. The alternative explanation suggested by Bertout et al. (1999), placing HR 5999/6000 in the background and unrelated to Lupus 3, seems highly unlikely in view of the central position of those stars in the area of the cloud, the frequent association of Herbig Ae/Be

stars with molecular clouds, and the resemblance of such an arrangement with that of other regions where the association between the Herbig Ae/Be stars and the clouds is made more obvious by reflection nebulosity, most notably the R Coronae Australis cloud. It is interesting to note that a recent independent determination of the distance to the Lupus clouds based on the moving cluster method carried out by Makarov (2007) also indicates a substantial depth ( $\sim 80$  pc) along the line of sight, and in particular a larger distance ( $\sim 175$  pc) of the classical T Tauri stars of the Lupus 3 cloud.

The currently available measurements discussed in this Section thus seem to hint to a depth of the complex of the same order as its angular extent on the plane of the sky, with varying distances to the different individual structures probably in the 140 to 200 pc range. The use of an average between those two values seems an acceptable compromise for most studies of the global properties of the complex. However, the likelihood that the different star forming clouds lie at sensibly different distances is a very important caveat in comparative studies of their associated stellar populations (see Section 6.). The use of a distance of 150 pc seems adequate for most of the clouds of the complex, but a value of 200 pc is likely to be more appropriate for Lupus 3.

#### 4. Molecular Gas and Dust

The molecular gas of the Lupus complex extends from the proximities of the Galactic plane ( $b \simeq +5^\circ$ ) to relatively high Galactic latitudes,  $b > +25^\circ$ . The large-scale structure shows an extended mass of gas at low latitudes, and several smaller, irregularly shaped clouds roughly distributed along an arc towards higher latitudes. Smaller clouds are also scattered among the dominant structures.

Even at the lowest latitudes the gas associated with the Lupus clouds is clearly distinguished from background gas by its positive LSR radial velocities, between 2 and 10 km s<sup>-1</sup>, which are forbidden by Galactic rotation in the direction of Lupus. This positive velocity, which is shared by the associated T Tauri stars (Dubath et al. 1996), is a distinctive feature of the Gould Belt, whose overall motion seems to be a composition of rotation and expansion (Comerón 1999).

The <sup>12</sup>CO survey of Murphy et al. (1986), covering approximately 170 square degrees at an angular resolution of 30', revealed for the first time the overall distribution of molecular gas over most of the Lupus complex. Murphy et al.'s map includes the clouds containing the T Tauri star associations previously known, and reveals the massive concentration at lower Galactic latitudes in whose outskirts the Lupus 3 and 4 clouds lie. Their map also hints at the continuation of the complex towards higher latitudes, although the mapped area is not large enough to fully encompass them. The molecular mass estimated by Murphy et al. (1986),  $3 \times 10^4 M_\odot$ , has often been adopted in other works. It is worth keeping in mind however that, as pointed out by the authors themselves, this is a highly uncertain value that may be incorrect by up to a factor of 2-3. The mass given above is actually an average between the mass inferred from the detected CO,  $1.5 \times 10^4 M_\odot$ , and the estimated virial mass of  $5 \times 10^4 M_\odot$ , assuming a distance of 130 pc to the complex.

Much recent progress in the mapping of the structure of the Lupus complex in molecular gas has been done with the Nagoya University's NANTEN 4m millimeter radiotelescope operating on the Las Campanas Observatory. Tachihara et al. (1996) mapped the Lupus 1, 2 and 3 clouds in <sup>13</sup>CO at a resolution of 8', as well as the densest regions of an additional cloud that they call Lupus 5, and which corresponds to the

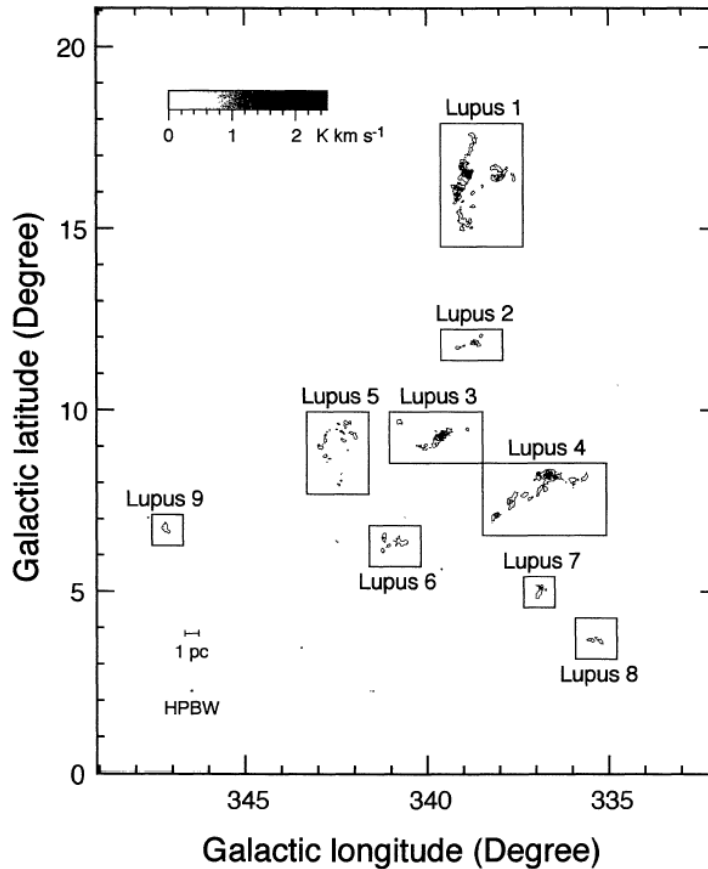


Figure 7. Overall view of the Lupus clouds as observed in  $C^{18}O$  emission, showing the distribution of the densest gas concentrations. From Hara et al. (1999).

densest region of the large concentration of molecular gas East (in Galactic coordinates) of Lupus 3. The  $^{13}CO$  survey was further extended in spatial coverage by Hara et al. (1999), who also carried out observations in the  $C^{18}O$  isotope, at a resolution of  $2''.7$ . Observations of Lupus 1, 2, 3, and 4 at  $48''$ , also in  $^{13}CO$  and  $C^{18}O$ , were carried out by Vilas-Boas et al. (2000), who list 36 condensations in the four clouds. A comparison between the distribution of dense cores and young stellar objects suggests a column density threshold of  $N(H_2) \simeq 6 \times 10^{21} \text{ cm}^{-2}$  for star formation.

The further extension of their survey towards the Galactic plane allowed Hara et al. (1999) to identify some new concentrations, labeled as Lupus 6 to 9, shown in Figure 7. Most of these concentrations appear as mere peaks in a widespread distribution of molecular gas in the  $^{12}CO$  maps (Tachihara et al. 2001), which has brought a certain confusion in current literature as to the precise structures to which these designations refer; compare e.g. Cambr esy (1999), Hara et al. (1999), and Tachihara et al. (2001).

A total molecular mass of  $4,500 M_{\odot}$  is estimated by Hara et al. (1999) for the dense gas ( $n(H_2) > 10^3 \text{ cm}^{-3}$ ; Tachihara et al. 2001) traced by the  $^{13}CO$  emission. The individual clouds have a very clumpy structure, best revealed by observations in the optically thin lines of  $^{13}CO$  and  $C^{18}O$  (Tachihara et al. 1996, 2001; Hara et al. 1999; see

Table 4). The parameters of the typical clump traced by  $C^{18}O$  are a mass  $M \simeq 9.7 M_{\odot}$  (with a range from 2 to  $40 M_{\odot}$ ) and a number density  $n(H_2) \simeq 6.1 \times 10^3 \text{ cm}^{-3}$  (with a range from  $3.5 \times 10^3 \text{ cm}^{-3}$  to  $1.1 \times 10^4 \text{ cm}^{-3}$ ), with caveats due to uncertainties in the excitation temperature (taken to be  $T_{\text{ex}} = 13 \text{ K}$  from the comparison to the optically thick  $^{12}CO$  emission, assuming LTE) and in the  $N(C^{18}O)/N(H_2)$  ratio, which is taken to be the same as derived by Tachihara et al. (2000) for the presumably similar Ophiuchus North region. The mass spectrum of the clumps follows a power law over the entire mass range above  $3 M_{\odot}$ , characterized by  $dN/dM \propto M^{-1.7 \pm 0.2}$ . As discussed by Hara et al. (1999), the power law index is similar to that of clumps traced by  $^{12}CO$  in other star forming regions (Yonekura et al. 1997). A higher scatter in the power law index exists for higher density clumps traced by  $C^{18}O$  or CS among different star forming regions. In that respect Hara et al. (1999) hint that the rather steep power law index might provide an explanation for the unusual fraction of late-type stars among the members of the T associations of Lupus as compared to other regions like Taurus, in which the power law index is close to  $-0.9$ .

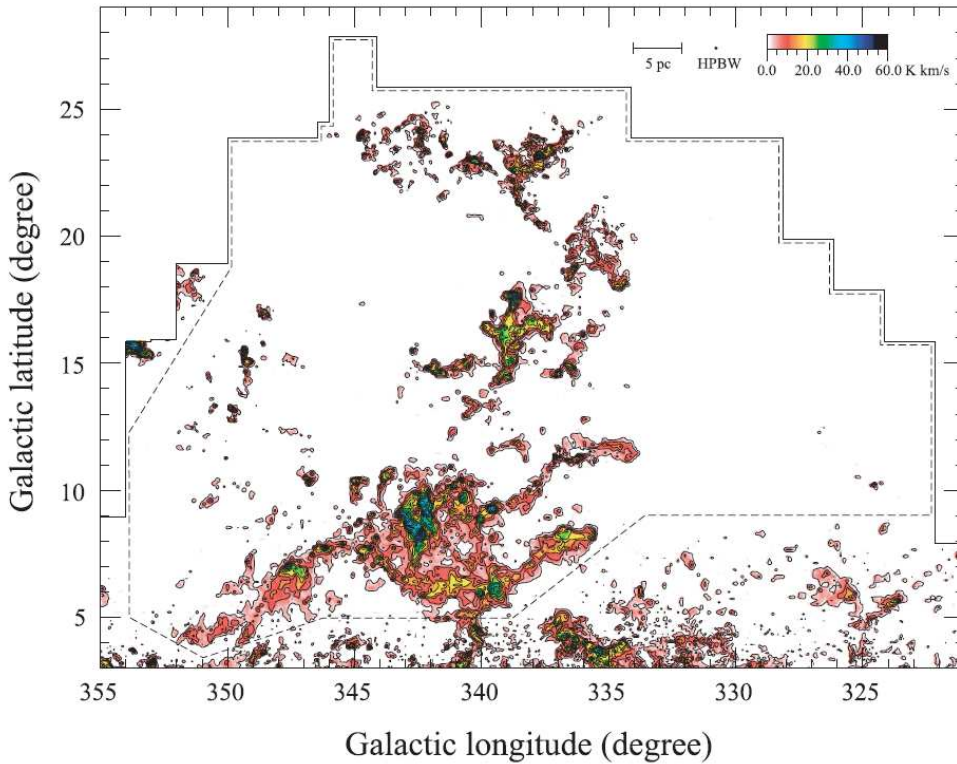


Figure 8.  $^{12}CO$  intensity map of the entire Lupus region. The major clouds are easily identified by comparison to Figure 9 after accounting for the different coordinate system. The emission at the lower border arises from the proximities of the Galactic plane, mostly in the background. From Tachihara et al. (2001).

Tachihara et al. (2001) mapped an area of 474 square degrees centered on the Lupus clouds at a resolution of  $4'$  or  $8'$  (depending on the position), thus improving on Murphy et al.'s work in both resolution and coverage (Figure 8). The total mass of the complex is found to be  $1.7 \times 10^4 M_{\odot}$ . Their study lists 105 individual clouds, using as

criteria for their definition the  $^{12}\text{CO}$  emission contour corresponding to  $5\sigma$  times their detection limit, rather than the identification of intensity peaks. Therefore, the largest of the clouds measured by Tachihara et al. (2001) contain multiple peaks, or clumps, as defined by other studies. The individual clouds observed by Tachihara et al. (2001) span a range in mass from about  $1 M_{\odot}$  to  $9.5 \times 10^3 M_{\odot}$ , following a mass distribution well approximated by a power law of the form  $dN/dM \propto M^{-1.37 \pm 0.13}$ . The largest cloud actually includes Lupus 3, 4, 5, and 6 as well as some secondary filamentary extensions, also detectable through the extinction they produce on the background. It contains more than half the mass of the complex, while Lupus 1, 2, and 9 are separated clouds (Lupus 7 and 8 of Hara et al. 1999 lie slightly outside the area mapped by Tachihara et al. 2001). The overall picture of the complex as traced by  $^{12}\text{CO}$  shows that the molecular gas distribution is dominated by clouds different from the "classical" Lupus 1 to 4, which stand out only due to their recent star forming activity.

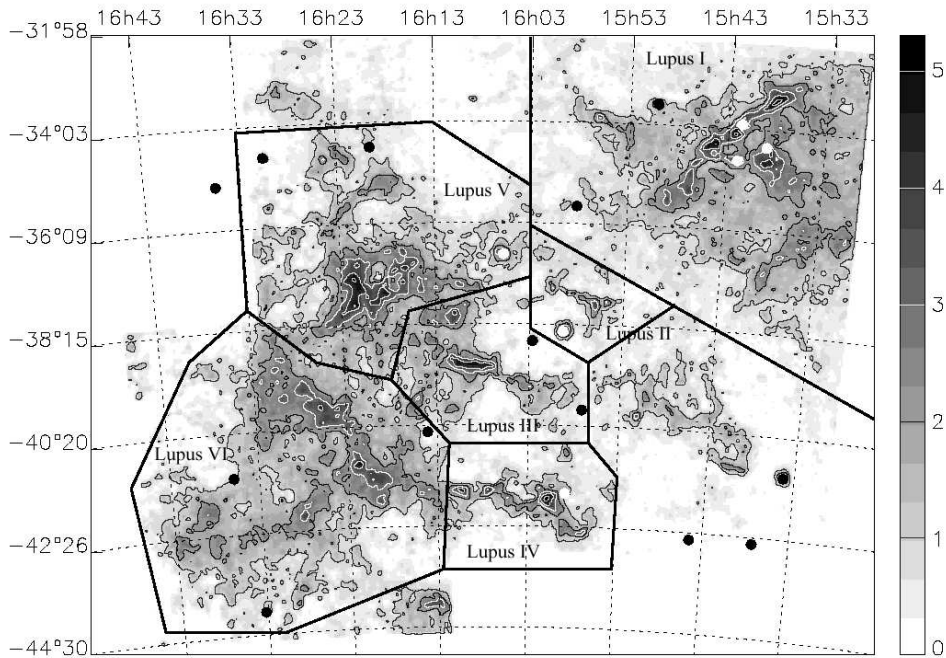


Figure 9. Grey-scale representation of the extinction derived from star counts, which outlines the distribution of gas in the entire Lupus region. The areas delimiting the major clouds are marked. Coordinates are in the J2000 equinox. From Cambr esy et al. (1999).

The overall structure of the interstellar medium in Lupus is also well traced by its associated dust, whose distribution can be derived from wide-area star counts. Cambr esy (1999) has produced detailed extinction maps for most nearby star forming regions and molecular clouds, including Lupus, based on star counts in the visible, using the USNO-PPM catalog (Figure 9). The choice of visible wavelengths allows the mapping of the dust distribution at small column densities, at the cost of decreased sensitivity in the densest areas of dark clouds that are best probed by infrared star counts (see e.g. Cambr esy et al. 1997). The extinction maps produced in this way, which bear a very close resemblance to the  $^{12}\text{CO}$  maps, can be translated into distributions of

mass by adopting an appropriate relationship between extinction and gas column density. Cambr esy (1999) has estimated peak extinctions towards the different clouds of the complex ranging from  $A_V \simeq 5.7$  to  $A_V \simeq 10.6$ , very similar to those derived by Dobashi et al. (2005). The pencil-beam estimates of extinction based on the reddening towards background stars indicates even larger values reaching up to  $A_V = 47$  in at least localized regions of the darkest areas of the Lupus 3 clouds (Nakajima et al. 2003). The total mass derived by Cambr esy (1999) is  $2.3 \times 10^4 M_\odot$ , which is probably an underestimate due to his adoption of the Knude & H og (1998) distance, 100 pc. The larger mass may be due to the sensitivity of visible star counts to even lower column densities and volume densities than  $^{12}\text{CO}$  maps, which probe gas with  $n(\text{H}_2) \simeq 100 \text{ cm}^{-3}$  and higher. A visual comparison of the CO maps of Tachihara et al. (2001) and the extinction maps of Cambr esy (1999) indeed shows that the clouds as traced by extinction extend beyond the boundaries traced by  $^{12}\text{CO}$  emission, and the interconnections among the different clouds of the complex by low column density bridges are clearly revealed. Star counts in the visible have also been used by Andreazza & Vilas-Boas (1996) to derive total masses in Lupus 1, 2, 3, and 4, which are interesting to compare with the masses derived by Hara et al. (1999) from the high-density tracer  $\text{C}^{18}\text{O}$ ; see Table 3. As one may expect, the mass traced by dust is higher, by a factor between 2 and 3, for Lupus 1, 2, and 3, due to the greater extension of the complex at low column densities. Nevertheless, similar values are obtained for Lupus 4. The comparison is more extreme in Lupus 6, for which the measurements by Hara et al. (1999) refer to the densest part of a vast cloud with several less prominent concentrations embedded in a common diffuse envelope, as seen in Cambr esy (1999). Given the strong differences in appearance and extent of this cloud when mapped in  $\text{C}^{18}\text{O}$  and in lower density tracers, we refer to the structure defined by Cambr esy (1999) as Lupus VI, keeping his nomenclature, and we reserve the denomination Lupus 6 for the high density peak in the  $\text{C}^{18}\text{O}$  map of Hara et al. (1999). Cambr esy’s Lupus VI cloud is actually as massive as Lupus 1, with a mass of  $2.3 \times 10^4 M_\odot$  if it is located at 150 pc. The possibility that this cloud, lying at low Galactic latitude ( $7^\circ < b < 10^\circ$ ) might actually be unrelated to the Lupus complex is disfavored by its radial velocity similar to that of other clouds in the complex (Tachihara et al. 2001).

A large-scale velocity gradient is seen throughout the complex, with radial velocities ranging between  $-4$  and  $+10 \text{ km s}^{-1}$ . The most negative velocities are seen at higher latitudes ( $b > 21^\circ$ ), while the gas at lower latitudes has mostly positive radial velocities that are forbidden for background gas in the same direction. Thus, the combination of position and kinematics provides a reliable criterion for identifying membership in the complex. Tachihara et al. (2001) point out that the clouds with negative velocities tend to be projected against the HI shell surrounding Upper Scorpius, suggesting that they may have been accelerated by it in our direction. They also note that the structure of such negative-velocity clouds tends to be clumpier, perhaps as a consequence of instabilities in the shell.

The molecular line widths are rather large. Hara et al. (1999) find a range of values between  $0.34 \text{ km s}^{-1}$  and  $1.79 \text{ km s}^{-1}$  with an average of  $0.90 \text{ km s}^{-1}$  for the  $\text{C}^{18}\text{O}$  cores. Similar results are found by Vilas-Boas et al. (2000), who remark on the similar properties of all the observed clouds in this regard. Hara et al. (1999) suggest turbulence, rather than rotation of the cores, as the cause of the observed line widths. Rotation of the clouds may be indicated by the observed average velocity gradients (Vilas-Boas et al. 2000) of  $0.1\text{-}0.2 \text{ km s}^{-1} \text{ pc}^{-1}$  in Lupus 2 and 4, and perhaps by the more complex pattern in Lupus 1 ( $0.3$  to  $0.7 \text{ km s}^{-1} \text{ pc}^{-1}$  depending on the measure-

Table 2. Features of the main Lupus clouds as traced by C<sup>18</sup>O

| #              | $l$   | $b$  | Sample members  | Notes  |
|----------------|-------|------|-----------------|--|
| 1              | 339°  | 16°5 | Sz 68<br>GQ Lup | Almost all TTS in low density regions<br>(Andreazza & Vilas-Boas 1996)   |
| 2              | 338°5 | 12°5 | RU Lup          | Two components separated by 1 km s <sup>-1</sup><br>with different <sup>13</sup> CO/ <sup>12</sup> CO<br>(Gahm et al. 1993)  |
| 3              | 339°5 | 9°5  | HR 5999/6000    | Densest T Tauri association (over 40 CTTS)<br>Most active star formation in the complex<br>Highest column density<br>Dense cores traced by H <sup>13</sup> CO <sup>+</sup><br>Probably farther than other clouds (Sect.3.) |
| 4              | 337°  | 8°   | RY Lup          | Few CTTS thus far, but H <sup>13</sup> CO <sup>+</sup> cores<br>suggest future star formation  |
| 5              | 342°5 | 9°   | IRAS 16133–3657 | No CTTS identified   |
| 6 <sup>1</sup> | 341°  | 6°   |                 | No star formation  |
| 7              | 337°  | 5°   |                 | No star formation  |
| 8              | 335°5 | 4°   |                 | No star formation  |
| 9              | 347°  | 6°5  |                 | No star formation  |
| VI             | 342°  | 8°   |                 | No star formation?   |

<sup>1</sup>: We refer to Lupus 6 as the peak mapped in C<sup>18</sup>O by Hara et al. (1999), which is embedded in the much larger and diffuse Lupus VI found in Cambr esy (1999) (see text).

ment baseline). No such gradients are observed in Lupus 3. The large line widths imply that the inferred core masses are much below their virial masses, a trend already found by Kawamura et al. (1998) in the Gemini-Auriga clouds. The line widths are also similar to those observed in Ophiuchus North (Tachihara et al. 2000), and about twice as high as those observed in the Taurus clouds. Other differences are noted with respect to the Taurus clouds by Hara et al. (1999), such as a smaller average core mass and H<sub>2</sub> column density.

It is tempting to interpret the similarities between Ophiuchus North and Lupus, and the differences between both clouds and the Taurus clouds, as due to the existence of nearby OB stars in the first two cases and their absence in the third. However, Hara et al. (1999) note that also the L1333 cloud in Cassiopeia (see chapter by Kun) is similar to Lupus (although a factor  $\sim 6$  smaller in total mass) but lacks nearby OB stars, indicating that the environment is not the only responsible factor for the different properties of clouds. Nevertheless, signs of the influence of the environment are discussed

Table 3. Projected sizes<sup>1</sup> and masses of main Lupus clouds from different tracers<sup>2</sup>

| Cloud | $\Delta l \times \Delta b$   | $M(A_V)^3$<br>( $M_\odot$ ) | $M(^{13}\text{CO})^4$<br>( $M_\odot$ ) | $M(\text{C}^{18}\text{O})^5$<br>( $M_\odot$ ) | $M_{\text{cond}}(A_V)^6$<br>( $M_\odot$ ) |
|-------|------------------------------|-----------------------------|--|---|---|
| 1     | $3^\circ \times 4^\circ$     | $2.6 \times 10^4$           | $1.3 \times 10^3$                      | 372   | 734                                       |
| 2     | $1.5^\circ \times 1^\circ$   | $2.0 \times 10^2$           | $1.1 \times 10^2$                      | 31  | 77  |
| 3     | $2^\circ \times 1^\circ$     | $3 \times 10^3$             | $3.4 \times 10^2$                      | 119   | 474                                       |
| 4     | $3^\circ \times 1^\circ 5$   | $1.6 \times 10^3$           |  | 246   | 257                                       |
| 5     | $2^\circ \times 3^\circ$     | $6.0 \times 10^3$           | $1.1 \times 10^3$                      | 57  |   |
| 6     | $1^\circ \times 1^\circ$     |                             | 7                                      |   |   |
| 7     | $1^\circ 5 \times 1^\circ 5$ |                             | 7                                      |   |   |
| 8     | $1^\circ \times 1^\circ$     |                             | 7                                      |   |   |
| 9     | $2^\circ \times 1^\circ 5$   |                             | 7                                      |   |   |
| VI    | $6^\circ \times 5^\circ$     | $2.6 \times 10^4$           |  |   |   |

<sup>1</sup>: Rough sizes from the  $^{12}\text{CO}$  contours (Tachihara et al. 2001)

<sup>2</sup>: All masses have been corrected to a distance of 160 pc

<sup>3</sup>: From Cambrésy et al. (1999)

<sup>4</sup>: From Tachihara et al. (1996)

<sup>5</sup>: From Hara et al. (1999)

<sup>6</sup>: Mass in dense condensations as derived from extinction, from Andreazza & Vilas-Boas (1996)

by Moreira & Yun (2002) in their detailed study of Lupus 2 and 4, where the distribution and properties of the molecular gas and dust are investigated. The emission in the 60 and 100  $\mu\text{m}$  IRAS bands can be interpreted as due to a single, cool dust component in equilibrium with the radiation field. The dust and gas are found to be well mixed, with the dust acting as a good tracer of molecular column density. With the caveats expressed by Moreira and Yun (2002) due to the fact that derived dust temperatures are emissivity-weighted towards warmer regions, the differences between the temperature distributions of gas (derived from  $^{12}\text{CO}$ ,  $^{13}\text{CO}$ , and  $\text{C}^{18}\text{O}$ ) and dust (from the intensity ratios at 60 and 100  $\mu\text{m}$ ) show that the gas is not heated only by dust, as the latter is hottest towards the edges of the clouds, where gas temperatures are lowest. This is interpreted as evidence for an external source of heating, which Moreira and Yun (2002) attribute to shocks driven by the expanding HI shells discussed above.

Detailed studies of the structure of Lupus 3 using complementary methods have been carried out by Teixeira et al. (2005) and by Tachihara et al. (2007). Using the near-infrared colors of background sources as a measure of column density, Teixeira et al. (2005) have mapped a wealth of small-scale structure, most notably five round cores with masses between 0.5 and 6  $M_\odot$  that they analyze by means of Bonnor-Ebert modeling. The stability analysis shows three of them to be stable and the other two unstable. Among the latter, one of them, discussed in more detail in Section 5., harbors signposts of star formation at far-infrared and millimeter wavelengths and is probably related to a Herbig-Haro object. The study also reveals a ring structure containing a loose aggregate of stars, which is interpreted as the remnants of the parental core of the aggregate. The extended emission of some of these cores is described by Nakajima et al. (2003), who find that their outer rims usually have enhanced  $J$ -band emission

Table 4. Individual cores<sup>1,2</sup> detected in C<sup>18</sup>O

| Cloud   | Core <sup>3</sup> | $l$<br>( $^{\circ}$ ) | $b$<br>( $^{\circ}$ ) | $\Delta V$<br>( $\text{km s}^{-1}$ ) | $N(\text{H}_2)$<br>( $10^{21} \text{ cm}^{-2}$ ) | $M$<br>( $M_{\odot}$ ) | $M_{\text{vir}}$<br>( $M_{\odot}$ ) | $R$<br>(pc) |
|---------|-------------------|-----------------------|-----------------------|--------------------------------------|--|------------------------|-------------------------------------|-------------|
| Lupus 1 | 11                | 337.57                | 16.37                 | 1.34                                 | 3.3  | 4                      | 55                                  | 0.15        |
|         | 13                | 337.90                | 16.47                 | 0.61                                 | 5.7  | 7                      | 10                                  | 0.13        |
|         | 15                | 338.10                | 16.70                 | 0.86                                 | 3.4  | 11                     | 33                                  | 0.21        |
|         | 17                | 338.70                | 17.47                 | 1.59                                 | 3.6  | 6                      | 83                                  | 0.16        |
|         | 18                | 338.73                | 16.00                 | 1.70                                 | 3.7  | 3                      | 63                                  | 0.11        |
|         | 19                | 338.77                | 17.23                 | 1.30                                 | 3.2  | 13                     | 83                                  | 0.23        |
|         | 20                | 338.83                | 16.53                 | 1.22                                 | 7.3  | 46                     | 93                                  | 0.30        |
|         | 21                | 339.03                | 15.00                 | 0.94                                 | 2.5  | 7                      | 35                                  | 0.19        |
|         | 22                | 339.03                | 16.70                 | 1.11                                 | 5.7  | 18                     | 55                                  | 0.21        |
|         | 24                | 339.13                | 15.47                 | 1.27                                 | 3.8  | 9                      | 64                                  | 0.19        |
|         | 25                | 339.13                | 15.93                 | 0.74                                 | 5.5  | 20                     | 27                                  | 0.22        |
| 26      | 339.13            | 16.10                 | 1.09                  | 5.4                                  | 30   | 69                     | 0.28                                |             |
| Lupus 2 | 16                | 338.67                | 11.87                 | 0.79                                 | 4.1  | 11                     | 27                                  | 0.20        |
|         | 23                | 339.13                | 11.73                 | 0.34                                 | 3.2  | 3                      | 3                                   | 0.12        |
| Lupus 3 | 27                | 339.57                | 9.33                  | 1.21                                 | 7.8  | 30                     | 71                                  | 0.23        |
|         | 29                | 340.73                | 9.67                  | 1.79                                 | 3.9  | 8                      | 111                                 | 0.17        |
| Lupus 4 | 3                 | 335.67                | 8.13                  | 0.60                                 | 3.5  | 6                      | 12                                  | 0.16        |
|         | 4                 | 335.97                | 8.07                  | 0.46                                 | 2.9  | 6                      | 7                                   | 0.17        |
|         | 5                 | 336.43                | 8.17                  | 0.46                                 | 4.7  | 13                     | 9                                   | 0.20        |
|         | 6                 | 336.67                | 8.20                  | 0.83                                 | 6.7  | 38                     | 41                                  | 0.29        |
|         | 7                 | 336.70                | 7.83                  | 0.89                                 | 2.8  | 7                      | 31                                  | 0.19        |
|         | 8                 | 336.83                | 7.87                  | 0.75                                 | 3.0  | 2                      | 13                                  | 0.11        |
|         | 10                | 336.90                | 8.23                  | 0.75                                 | 4.5  | 7                      | 17                                  | 0.15        |
|         | 12                | 337.70                | 7.50                  | 0.71                                 | 4.2  | 24                     | 30                                  | 0.29        |
| 14      | 338.10            | 7.10                  | 0.50                  | 5.2                                  | 8  | 7                      | 0.15                                |             |
| Lupus 5 | 33                | 341.97                | 9.27                  | 0.61                                 | 3.0  | 6                      | 13                                  | 0.17        |
|         | 34                | 342.80                | 8.73                  | 0.86                                 | 3.4  | 3                      | 18                                  | 0.12        |
|         | 35                | 342.93                | 9.00                  | 1.23                                 | 3.2  | 4                      | 47                                  | 0.15        |
| Lupus 6 | 28                | 340.67                | 6.33                  | 0.52                                 | 3.0  | 10                     | 12                                  | 0.21        |
|         | 30                | 341.07                | 6.27                  | 0.84                                 | 2.7  | 2                      | 17                                  | 0.12        |
|         | 31                | 341.20                | 6.13                  | 0.91                                 | 3.0  | 4                      | 26                                  | 0.15        |
|         | 32                | 341.20                | 6.50                  | 0.51                                 | 4.1  | 8                      | 9                                   | 0.17        |
| Lupus 7 | 9                 | 336.87                | 5.07                  | 0.57                                 | 4.6  | 6                      | 9                                   | 0.13        |
| Lupus 8 | 1                 | 335.23                | 3.63                  | 0.89                                 | 3.1  | 3                      | 21                                  | 0.13        |
|         | 2                 | 335.50                | 3.67                  | 0.75                                 | 3.6  | 2                      | 13                                  | 0.11        |
| Lupus 9 | 36                | 347.23                | 6.73                  | 0.99                                 | 3.4  | 14                     | 49                                  | 0.13        |

<sup>1</sup>: From Hara et al. (1999)<sup>2</sup>: Masses, volume densities, and radii corrected to a distance of 160 pc<sup>3</sup>: Core number from Hara et al. (1999)

whereas most of the cores glow faintly in the  $K$  band, resulting from the scattering of the ambient starlight by dust.

A region roughly coincident with that observed by Teixeira et al. (2005) has been mapped in the  $\text{H}^{13}\text{CO}^+$  high density tracer by Tachihara et al. (2007) as well as at the

wavelength of 1.2 mm that is expected to trace thermal emission by dust. Some of the cores identified in the extinction mapping are also retrieved in  $\text{H}^{13}\text{CO}^+$  and millimeter continuum emission, but their degree of prominence is quite different: the very opaque cores C and D of Teixeira et al. (2005) are faint in  $\text{H}^{13}\text{CO}^+$ , whereas their cores B and E, which produce only moderate extinction on the background in the maps of Teixeira et al. (2005), are prominent in  $\text{H}^{13}\text{CO}^+$  emission and are connected by a bridge that is unseen in the extinction mapping. Conversely, the extinction bridge connecting cores A and E does not have a  $\text{H}^{13}\text{CO}^+$  counterpart. Finally, it is remarkable that no  $\text{H}^{13}\text{CO}^+$  emission is detected on the western part of the cloud, where extinction mapping does reveal some cores.

#### 4.1. Magnetic Fields

Magnetic field measurements in the main Lupus clouds have been carried out by several authors, based on optical polarization of the light of stars observed towards and around them. Observations of Lupus 1, 2, 3, and 4 by Vrba et al. (1992) have been reported by Myers & Goodman (1991), who discussed and modeled the observed trends in the ordering of the magnetic field lines. A sample of clouds including Lupus and other clouds was separated into two classes characterized by the presence or absence of embedded clusters. In this scheme, Lupus 3 belongs to the first class, and Lupus 1, 2, and 4 to the second. Overall, it is found that clouds containing clusters tend to have a more disordered magnetic field pattern, which is thought to be related to the presence of young stars and, more importantly, dense gas. This trend is roughly present among the four Lupus clouds included in Myers and Goodman's (1991) sample, but not rigorously. Lupus 4 does show a single mean direction all over its extension, with a small and spatially uniform dispersion. However, Lupus 1 and 2 are among the clouds without embedded clusters having the largest magnetic field direction dispersion, and both have more complex magnetic field patterns. Lupus 2 contains two zones with different dispersions, in which only the low-dispersion zone has a magnetic field along a definite direction. On the other hand, Lupus 3 has only a moderate dispersion of the directions of the magnetic field lines and, like Lupus 1, has separate zones with clearly different directions. As Vrba et al. (1992) point out, the polarization direction in all four clouds tends to be perpendicular to their elongation, suggesting collapse of the clouds along the magnetic field lines. Krautter (1991) went on to suggest that such observations may lend support to the idea that star formation in the Lupus clouds has proceeded under subcritical conditions (Shu et al. 1987), in which magnetic fields provide effective support against collapse leading to the preferential formation of low mass stars. However, Andreatta & Vilas-Boas (1996) note that this relationship ceases to apply at the level of the individual cores that these clouds contain, whose orientations seems to be independent of that of the magnetic field at their positions, thus casting doubts on such interpretation.

Detailed optical polarization observations of stars towards and around Lupus 1 and 4 have been presented by Rizzo et al. (1998). In agreement with earlier results by Myers & Goodman (1991), they find that Lupus 4 has a well-ordered magnetic field roughly perpendicular to the filament axis, suggesting that collapse has proceeded along the magnetic field lines. The field in the surrounding area, derived from background stars lying farther from the darkest areas of the cloud, is in a similar direction. The pattern is however more complex in Lupus 1, where a clear variation is observed in the magnetic field orientation across the cloud, and also between the cloud and its surroundings,

which seems to indicate a rather complex cloud formation process. Furthermore, Rizzo et al. (1998) reexamine the conclusion of Andreazza & Vilas-Boas (1996) regarding the orientation of condensations, and find large variations in the magnetic field orientation not only among different condensations, but also within one single condensation. Such variations are not observed however among the condensations of Lupus 4, where the polarization vectors are highly uniform in direction.

## 5. Infrared Sources and Outflows

The most luminous candidate protostellar objects in Lupus have been identified by the InfraRed Astronomical Satellite (IRAS) as point sources having a cold or warm spectral energy distribution between 12 and 60  $\mu\text{m}$ . Tachihara et al. (1996) list 9 such sources lying within or near the concentrations of their  $^{13}\text{CO}$  maps, and report on a molecular outflow associated with one of them, IRAS15398–3359 in Lupus 1, with a dynamical timescale of  $\sim 2000$  years and an approximate mass of  $7 \times 10^{-4} M_{\odot}$ .  $\text{HCO}^+$  observations indicate that the central source, whose bolometric luminosity is  $\sim 1.2 L_{\odot}$ , could be in the protostellar collapse phase (Shirley et al. 2000). Its counterpart in the visible is an extended nebula, HH 185, whose spectrum shows the signatures of shock excitation (Heyer & Graham 1989). These authors also identify three other shock-excited nebulae in Lupus 1, notably the ones associated with Sz 68 and Sz 69 (HH 186, HH 187).

Using the same color criteria of Tachihara et al. (1996) for the selection of protostellar candidates in the IRAS Point Source Catalog, extending them to the entire area of the Lupus clouds rather than to the selected regions mapped by those authors, we identify the 18 sources listed in Table 5. The color criteria are  $\log(F_{12}/F_{25}) < 0$ ,  $\log(F_{25}/F_{60}) < 0.3$ , where  $F_{\lambda}$  is the flux density at the wavelength of  $\lambda$  microns. Four sources, IRAS 16032–3537, IRAS 16097–3606, IRAS 16280–4008, and IRAS 16342–3814 are excluded as they are identified as the planetary nebulae WR72, NGC 6072, and NGC 6153, and the post-AGB star OH 344.07+5.84, respectively. As a cross-identification shows, the criterion also selects the dusty envelopes of visible classical T Tauri stars.

The core associated with the faint IRAS source 16054–3857 (not selected by the criteria used to produce Table 5) has received recent attention as a likely low-luminosity protostar. It is detected in the extinction mapping of Nakajima et al. (2003) and Teixeira et al. (2005) (their core C; see Section 4.), who derived a mass of 5–10  $M_{\odot}$  and inferred that it is gravitationally unstable from their Bonnor-Ebert analysis. The detection of the source at 1.2 mm (Tachihara et al. 2007), the combination of the flux at that wavelength with that measured by IRAS at 60  $\mu\text{m}$  and its non-detection at other IRAS bands suggest a temperature  $T \simeq 33$  K and  $L \simeq 0.6 L_{\text{bol}}$  (the latter assuming a distance of 200 pc). The Herbig-Haro object HH 78, discovered by Reipurth & Graham (1988), is close to it and probably related either to this source or to the neighboring core D (Teixeira et al. 2005). Near-infrared images also show a wisp of nebulosity extending radially from the center of the core. The wisp is not detected in narrow-band images centered on the  $\text{H}_2 S(1) v = 1 \rightarrow 0$  line at 2.122  $\mu\text{m}$ , suggesting that it may be produced by reflection in the walls of a cavity previously carved by a jet from the central protostar and having an unimpeded line of sight towards the central object, rather than by shocked gas. IRAS 16054–3857 thus displays many of the characteristics of a low-luminosity Class 0 source (André et al. 1993), representing the earliest protostellar phases.

Table 5. Candidate protostellar objects in the IRAS Point Source Catalog

| IRAS Object | $F_{12\mu\text{m}}$ | $F_{25\mu\text{m}}$ | $F_{60\mu\text{m}}$ | Cloud   | Associated objects |
|-------------|---------------------|---------------------|---------------------|---------|--------------------|
| 15398–3359  | 0.25                | 1.28                | 15.2                | Lupus 1 | HH 185             |
| 15420–3408  | 2.59                | 3.98                | 7.92                | Lupus 1 | HT Lup             |
| 15448–3506  | 0.91                | 1.97                | 1.95                | Lupus 1 | HN Lup             |
| 15459–3529  | 0.87                | 1.22                | 1.88                | Lupus 1 | GQ Lup             |
| 15528–3747  | 0.66                | 1.00                | 1.55                | Lupus 2 | IM Lup             |
| 15532–4210  | 10.3                | 21.2                | 105                 | Lupus 4 |                    |
| 15534–3740  | 0.24                | 4.54                | 4.97                | Lupus 2 | RU Lup             |
| 15561–4013  | 1.50                | 2.83                | 5.61                | Lupus 3 | RY Lup             |
| 15573–4147  | 0.28                | 0.77                | 1.17                | Lupus 4 | MY Lup             |
| 15597–4010  | 0.80                | 1.10                | 1.24                | Lupus 3 | EX Lup             |
| 16017–3936  | 0.76                | 1.60                | 9.50                | Lupus 3 |                    |
| 16064–3903  | 0.38                | 0.54                | 0.60                | Lupus 3 |                    |
| 16244–4031  | 1.41                | 1.43                | 1.27                | Lupus 6 |                    |
| 16245–3859  | 3.78                | 25.2                | 31.6                | Lupus 5 |                    |
| 16280–3435  | 0.66                | 1.20                | 1.29                | Lupus 5 | N Sco              |
| 16342–3555  | 1.71                | 1.81                | 1.48                | Lupus 5 |                    |
| 16346–3536  | 0.36                | 0.81                | 0.70                | Lupus 5 |                    |

Table 6. Herbig-Haro objects in Lupus<sup>1</sup>

| Object | RA (2000)  | Dec (2000) | Associated object | Cloud   |
|--------|------------|------------|-------------------|---------|
| HH 185 | 15 43 01.5 | –34 09 16  | IRAS 15398–3359   | Lupus 1 |
| HH 186 | 15 45 12.7 | –34 17 30  | Sz 68             | Lupus 1 |
| HH 187 | 15 45 18.6 | –34 17 32  | Sz 68/69          | Lupus 1 |
| HH 55  | 15 56 36.7 | –37 50 52  | near RU Lup       | Lupus 2 |
| HH 228 | 16 08 29.4 | –39 03 11  | Th 28             | Lupus 3 |
| HH 78  | 16 09 12.8 | –39 05 02  |                   | Lupus 3 |
| HH 600 | 16 08 15.9 | –39 05 31  | Par-Lup3-4        | Lupus 3 |

<sup>1</sup>: Data from Reipurth (2000), except for HH 600. The designation of HH 600 is from B. Reipurth, priv. comm.

Table 7. Possible new Herbig-Haro objects identified with Spitzer (Merín et al. 2008)

| RA (2000)   | Dec (2000)  | Associated object | Cloud   |
|-------------|-------------|-------------------|---------|
| 15 38 48.36 | –34 40 38.2 | IRAS 15356-3430   | Lupus 1 |
| 16 10 57.95 | –38 04 37.9 | –                 | Lupus 3 |
| 16 00 39.04 | –42 06 51.5 | –                 | Lupus 4 |

In addition to HH 78, several other Herbig-Haro outflows are known in Lupus 1, 2, and 3 (Table 6), most of them associated with well known young stellar objects. The driving source of HH 55 is not the nearby RU Lup, as the morphology of the jet leads one to suspect at first sight, but rather a very low luminosity object in its proximity (Graham & Chen 1994); see Section 7.2.

A recent addition to the cataloged Herbig-Haro outflows is the faint and small jet reported by Fernández & Comerón (2005), which is associated with the very low luminosity star Par-Lup3-4 and is prominent when observed through a [SII] filter; more details are given in Section 7.6.. Finally, three nebulous objects with appearances resembling Herbig-Haro objects have been noticed in Spitzer images by Merín et al. (2008). They are tentatively listed in Table 7, as their spectroscopic confirmation is pending at the moment.

## 6. The Stellar Population

Even though only low-mass stars are formed in the Lupus complex, considerable variety is displayed in the clustering degree found among the different clouds, which ranges from one of the densest T Tauri associations known (Lupus 3), to isolated or sparse star formation (e.g. Lupus 1), to virtually no star formation (Lupus 5). The study of the embedded stellar population is facilitated thanks to the much lower intervening extinction, which in general does not exceed  $A_V \simeq 10$  mag (Cambrésy 1999), thus making virtually all the Lupus members accessible to studies in the visible spectral range. By contrast,  $A_V \sim 50$  mag are not rare in  $\rho$  Oph, reaching up to  $\sim 200$  mag in the densest regions (see Wilking et al.'s chapter in this volume).

Early studies leading to the identification of the classical T Tauri stars (CTTS) in Lupus have been noted in the Introduction. The most extensive list of CTTS to the date is still the one of H $\alpha$ -emitting members produced by Schwartz (1977), after the revision by Krautter et al. (1991) and Hughes et al. (1994) who found that a few of the objects are not actually displaying H $\alpha$  emission, but are mostly background giants. In addition, some of the emission-line objects reported in that study have been shown to be unrelated to the clouds: measured radial velocities measured for Sz 85, 87, and 89 by Dubath et al. (1996) show them to be background objects. The list of candidate members of the Lupus complex has been greatly expanded by the discovery of large numbers of weak-line T Tauri stars (WTTS) in the ROSAT All-Sky Survey (Krautter et al. 1997), but the census of CTTS is still restricted to Lupus 1, 2, 3, and 4; see Tables 10, 11, and 12. Furthermore, the physical association between most WTTS and the Lupus clouds is doubtful, as explained in Section 6.6. No obvious signatures of recent or ongoing star formation are detected in Lupus 5 or 6, with the possible exception the low-luminosity source IRAS 16133–3657 in Lupus 5. No classical T Tauri stars are identified in these clouds by their X-ray emission in the ROSAT All-Sky Survey (Krautter et al. 1997), although CTTS, which are weak X-ray emitters, may have been missed at the sensitivity of the survey.

The overall kinematics of the stellar population of the Lupus clouds has been recently discussed by Makarov (2007) making use of the UCAC2 catalogue. In addition to the evidence for depth and for a greater distance of Lupus 3 already discussed in Section 3., Makarov (2007) reports a remarkably uniform streaming motion for the entire complex with an internal one-dimensional velocity dispersion of only  $1.3 \text{ km s}^{-1}$  and hints of expansion. The latter is highly insufficient to account for the current vol-

ume occupied by the clouds if they expanded from an originally small region, given the young age of its members.

A first systematic search for binary stars in Lupus 1, 2 and 3 was carried out by Reipurth & Zinnecker (1993), who found 8 binaries among their 59 targets with separations between  $1''$  and  $12''$  (150 to 1800 AU at their assumed distance of 150 pc). The study was extended by Ghez et al. (1997), who observed also objects in Lupus 4 and carried out their observations at  $2.2 \mu\text{m}$ , thus being sensitive to cool companions too faint to be detected in the  $I$  band used by Reipurth & Zinnecker (1993). Furthermore, they used speckle interferometry to extend the range of separations probed down to  $0.1''$ . The resulting binary fraction in the  $1'' - 12''$  range turns out to be 0.3 for the 33 objects observed in the infrared. They also detected 2 more companions at less than  $1''$  from 16 of these objects, implying at least a binary fraction of  $\sim 0.37$  in the  $0''.1-12''.0$  separation range, which may rise up to near 0.5 after correcting for close companions undetected due to the flux contrast with the primary (see discussion in Ghez et al. 1997). This is about twice as high as the binary fraction in the field, a result commonly found also in other low mass star forming regions. The statistics have been recently expanded with the Spitzer-based work of Merín et al. (2008), who identified visual binaries with separations between  $1''$  and  $10''$  among the new members identified by their mid-infrared excess. The larger size of their sample results in the identification of many more binary or multiple systems (see Table 9). The overall binary fraction derived by Merín et al. (2008) is 0.35 consistent with those found by Ghez et al. (1997) despite the insensitivity to the closest systems.

Table 8. Binary stars in the Lupus clouds (From Reipurth & Zinnecker 1993 and Ghez et al. 1997)

| Star     | Flux ratio | Separation | Cloud   |
|----------|------------|------------|---------|
| Sz 65/66 | 3.10       | $6''5$     | Lupus 1 |
| Sz 68    | 6          | $0''107$   | Lupus 1 |
| Sz 74    | 2.4        | $0''24$    | Lupus 1 |
| Sz 77    | 2.7        | $1''8$     | Lupus 1 |
| Sz 81    | 1.80       | $1''99$    | Lupus 2 |
| Sz 88    | 5.7        | $1''49$    | Lupus 3 |
| Sz 91    | 9          | $8''7$     | Lupus 3 |
| HR 5999  | 35         | $1''53$    | Lupus 3 |
| Sz 105   | 70         | $10''9$    | Lupus 3 |
| Sz 120   | 9.6        | $2''7$     | Lupus 3 |
| Sz 123   | 44         | $1''7$     | Lupus 3 |

### 6.1. The Initial Mass Function

The dominance of late-type stars in Lupus as compared to other low-mass star forming regions was already noted by Appenzeller et al. (1983) and has been confirmed by other studies since then (Hughes et al. 1994). Indeed, M-type stars are more abundant in Lupus when compared to K-type pre-main sequence stars than in the Taurus star forming clouds, which is in better agreement with the Initial Mass Function (IMF) in the field. The statistical evidence for IMF differences between Taurus and Lupus has

Table 9. New binary stars in the Lupus clouds, from Merín et al. (2008)

| Star                    | Separation           | Cloud   |
|-------------------------|----------------------|---------|
| SSTc2d J153803.1-331358 | 6''0                 | Lupus 1 |
| AKC2006-18              | 8''4 and 8''5        | Lupus 1 |
| Sz69                    | 6''6                 | Lupus 1 |
| SSTc2d J154518.5-342125 | 6''1 and 6''2        | Lupus 1 |
| SSTc2d J160703.9-391112 | 12''0                | Lupus 3 |
| SSTc2d J160708.6-391407 | 2''2                 | Lupus 3 |
| SSTc2d J160708.6-394723 | 2''9                 | Lupus 3 |
| Lup713                  | 3''2                 | Lupus 3 |
| Sz 95                   | 3''0                 | Lupus 3 |
| 2MASS J16075475-3915446 | 2''2                 | Lupus 3 |
| SSTc2d J160755.3-390718 | 2''7                 | Lupus 3 |
| SSTc2d J160803.0-385229 | 6''0                 | Lupus 3 |
| Sz 100                  | 4''0                 | Lupus 3 |
| Lup607                  | 2''5                 | Lupus 3 |
| Sz 108/108B             | 3''8                 | Lupus 3 |
| IRAC J16084679-3902074  | 4''0                 | Lupus 3 |
| 2MASS J16084747-3905087 | 2''2 and 5''2        | Lupus 3 |
| Par-Lup3-4              | 4''5                 | Lupus 3 |
| 2MASS J16085373-3914367 | 5''0                 | Lupus 3 |
| 2MASS J16085529-3848481 | 3''0                 | Lupus 3 |
| Sz 112                  | 2''8                 | Lupus 3 |
| NTO2000-0537.4-5653     | 5''0                 | Lupus 3 |
| 2MASS J16085953-3856275 | 2''0                 | Lupus 3 |
| NTO2000-0540.9-5757     | 2''4 and 2''4        | Lupus 3 |
| Lup710                  | 3''4                 | Lupus 3 |
| NTO2000-0601.7-5616     | 7''0                 | Lupus 3 |
| NTO2000-614.0-5414      | 0''8, 1''5, and 2''3 | Lupus 3 |
| Sz 116                  | 1''5                 | Lupus 3 |
| Lup810s                 | 2''2 and 2''0        | Lupus 3 |
| Lup818s                 | 1''9                 | Lupus 3 |
| SSTc2d J161013.1-384617 | 3''0 and 3''0        | Lupus 3 |
| SSTc2d J161018.6-383613 | 2''7                 | Lupus 3 |
| SSTc2d J161019.8-383607 | 3''9                 | Lupus 3 |
| SSTc2d J161118.7-385824 | 10''0                | Lupus 3 |
| SST-Lup3-1              | 10''0                | Lupus 3 |
| SSTc2d J161200.1-385557 | 4''0                 | Lupus 3 |
| SSTc2d J161211.2-383220 | 2''7                 | Lupus 3 |
| SSTc2d J161218.5-393418 | 1''7                 | Lupus 3 |
| SSTc2d J161344.1-373646 | 4''2                 | Lupus 3 |
| SSTc2d J155945.3-415457 | 4''0                 | Lupus 4 |
| SSTc2d J160000.6-422158 | 6''0                 | Lupus 4 |
| SSTc2d J160002.4-422216 | 9''0                 | Lupus 4 |
| SSTc2d J160026.1-415356 | 2''8 and 3''9        | Lupus 4 |
| Sz 130                  | 3''7 and 6''8        | Lupus 4 |
| SSTc2d J160129.7-420804 | 2''3                 | Lupus 4 |
| IRAS 15589-4132         | 2''6                 | Lupus 4 |
| Sz 133                  | 3''6                 | Lupus 4 |

Table 10. Classical T Tauri stars in Lupus 1 and 2

| Star       | $\alpha(2000)$ | $\delta(2000)$ | Sp. type <sup>1</sup> | Other names <sup>2</sup>   |
|------------|----------------|----------------|-----------------------|--|
| In Lupus 1 |                |                |                       |  |
| Sz 65      | 15 39 27.8     | -34 46 17      | M0                    | IK Lup   |
| Sz 66      | 15 39 28.3     | -34 46 18      | M3                    | -  |
| Sz 67      | 15 40 38.3     | -34 21 36      | M4                    | KWS97 Lupus 1-11   |
| Sz 68      | 15 45 12.9     | -34 17 31      | K2                    | HT Lup, Hip 77157,<br>KWS97 Lup 1-28, Th 1, Hen 3-1095,<br>1RXS J154513.6-341733 |
| Sz 69      | 15 45 17.4     | -34 18 28      | M1                    | HW Lup, Hen 3-1096, Th 2   |
| Sz 70      | 15 46 43.0     | -34 30 12      | M5                    | -  |
| Sz 71      | 15 46 44.7     | -34 30 35      | M2                    | GW Lup, Hen 3-1097, Th 3   |
| Sz 72      | 15 47 50.6     | -35 28 35      | M3                    | HM Lup, Hen 3-1101, Th 4   |
| Sz 73      | 15 47 56.9     | -35 14 35      | M0                    | Th 5, KWS97 Lup1-48  |
| Sz 74      | 15 48 05.2     | -35 15 53      | M1.5                  | HN Lup, Hen 3-1104, Th 6   |
| Sz 75      | 15 49 12.1     | -35 39 04      | K7-M0                 | GQ Lup, Hen 3-1106,<br>KWS97 1-56, Th 7  |
| Sz 76      | 15 49 30.8     | -35 49 52      | M1                    | KWS97 Lup1-59  |
| Sz 77      | 15 51 47.0     | -35 56 43      | M0                    | KWS97 Lup1-68  |
| In Lupus 2 |                |                |                       |  |
| Sz 79      | 15 53 42.7     | -38 08 11      |                       | -  |
| Sz 80      | 15 55 05.7     | -38 03 22      |                       | -  |
| Sz 81      | 15 55 50.2     | -38 01 33      | M5.5                  | KWS97 Lup2-20, Th 10   |
| Sz 82      | 15 56 09.2     | -37 56 06      | M0                    | IM Lup, HIP 78053,<br>Th 12, KWS97 Lup2-24,<br>1RXS J155609.3-375556             |
| Sz 83      | 15 56 42.3     | -37 49 15      | K7-M0                 | RU Lup, HIP 78094,<br>KWS97 Lup2-29, Hen 3-1120, Th 13                           |
| Sz 84      | 15 58 02.5     | -37 36 03      | M5.5                  | -  |

<sup>1</sup>: Spectral types from Hughes et al. (1994).<sup>2</sup>: Catalog denominations: *Th*: Thé (1962); *KWS97*: Krautter et al. (1997)

been studied in detail by Hughes et al. (1994). Differences between the medians of the mass spectra in Taurus and Lupus are found at the 95% significance level, in the sense of the median mass in Lupus being lower. The peak in mass is found to be similar among the Lupus, Taurus, and Chamaeleon regions, but Lupus is characterized by a tail towards lower masses and a sharp drop at  $M > 0.5 M_{\odot}$ , this latter value being based on the D'Antona & Mazzitelli (1994) evolutionary tracks. These features seem to be common to all the star-forming clouds in Lupus, as shown by Hughes et al. (1994) by comparing the mass histograms for Lupus 1 and 2 on one side, and Lupus 3 on the other. Nevertheless, it appears unlikely that such a trend continues towards spectral types later than mid-M and into the brown dwarf realm. The small number of objects newly identified in a deep survey of 1.6 square degrees of Lupus 3 by López Martí et al. (2005) (see Section 6.4.) and tentatively classified as later than M6 suggests that the abundance of very low mass stars of mid-M types may be caused by a peak in the

Table 11. Classical T Tauri stars in Lupus 3

| Star    | $\alpha(2000)$ | $\delta(2000)$ | Sp. type <sup>1</sup> | Other names <sup>2</sup>                       |
|---------|----------------|----------------|-----------------------|--|
| Sz 78   | 15 53 41.2     | -39 00 38      | -                     |  |
| RY Lup  | 15 59 28.4     | -40 21 51      | K4                    | HIP 78317                                      |
| EX Lup  | 16 03 05.5     | -40 18 26      | M0                    | HD 325367, Th 14                               |
| Sz 86   | 16 06 44.3     | -39 14 11      |                       | Th 16  |
| Sz 88   | 16 07 00.6     | -39 02 19      | M1                    | HO Lup, KWS Lup 3-22,<br>Hen 3-1140, Th 18     |
| Sz 90   | 16 07 10.1     | -39 11 03      | K7-M0                 | KWS97 Lup 3-23, Th 21                          |
| Sz 91   | 16 07 11.6     | -39 03 47      | M0.5                  | KWS Lup 3-24, Th 20                            |
| Sz 92   | 16 07 15.2     | -40 03 42      |                       | Th 22  |
| Sz 93   | 16 07 17.8     | -39 34 05      |                       | Th 23  |
| Sz 94   | 16 07 49.6     | -39 04 29      | M4                    | KWS97 Lup3-28                                  |
| Sz 95   | 16 07 52.3     | -38 58 06      | M1.5                  | -  |
| Sz 96   | 16 08 12.6     | -39 08 33      | M1.5                  | KWS97 Lup2-31                                  |
| Sz 97   | 16 08 21.8     | -39 04 22      | M3                    | Th 24  |
| Sz 98   | 16 08 22.5     | -39 04 46      | M0                    | HK Lup   |
| Sz 99   | 16 08 24.1     | -39 05 50      | M3.5                  | Th 25  |
| Sz 100  | 16 08 25.8     | -39 06 01      | M5                    | Th 26  |
| Sz 101  | 16 08 28.4     | -39 05 32      | M4                    | Th 27  |
| Sz 102  | 16 08 29.7     | -39 03 11      | K0                    | Krautter's star, Th 28                         |
| Sz 103  | 16 08 30.3     | -39 06 11      | M4                    | Th 29  |
| Sz 104  | 16 08 30.8     | -39 05 49      | M5                    | Th 30  |
| HR 5999 | 16 08 34.3     | -39 06 18      | A7                    | V856 Sco, HD 144668                            |
| HR 6000 | 16 08 34.6     | -39 05 34      | A3                    | HIP 79081, KWS97 Lup3-40, V1027 Sco            |
| Sz 105  | 16 08 37.0     | -40 16 21      | M4                    | Th 31  |
| Sz 106  | 16 08 39.7     | -39 06 26      | M0                    | -  |
| Sz 107  | 16 08 41.8     | -39 01 36      | M5.5                  | KWS97 Lup3-44                                  |
| Sz 108  | 16 08 42.7     | -39 06 18      | M1                    | KWS97 Lup 3-45                                 |
| Sz 109  | 16 08 48.2     | -39 04 19      | M5.5                  | -  |
| Sz 110  | 16 08 51.6     | -39 03 18      | M2                    | Th 32  |
| Sz 111  | 16 08 54.7     | -39 37 44      | M1.5                  | Th 33, KWS Lup3 49, Hen 3-1145                 |
| Sz 112  | 16 08 55.5     | -39 02 35      | M4                    | -  |
| Sz 113  | 16 08 57.8     | -39 02 23      | M4                    | Th 34  |
| Sz 114  | 16 09 01.9     | -39 05 12      | M4                    | V908 Sco, KWS97 Lup3 50, Th 35                 |
| Sz 115  | 16 09 06.2     | -39 08 52      | M4                    | -  |
| Sz 116  | 16 09 42.6     | -39 19 42      | M1.5                  | KWS97 Lup 3-58, Th 36                          |
| Sz 117  | 16 09 44.3     | -39 13 30      | M2                    | Th 37  |
| Sz 118  | 16 09 48.7     | -39 11 17      | K6                    | -  |
| Sz 119  | 16 09 57.1     | -38 59 48      | M4                    | KWS97 Lup3 60, Th 38                           |
| Sz 120  | 16 10 10.6     | -40 07 44      | B4                    | HIP 79230, Hen 3-1149, Th 39,<br>KWS97 Lup3-62 |
| Sz 121  | 16 10 12.2     | -39 21 19      | M3                    | KWS97 Lup3-63, Th 40                           |
| Sz 122  | 16 10 16.4     | -39 08 01      | M2                    | KWS97 Lup3 64, Th 41                           |
| Sz 123  | 16 10 51.5     | -38 53 14      | M1                    | Th 42  |
| Sz 124  | 16 11 53.4     | -39 02 16      | K7-M0                 | KWS97 Lup3 78, Th 43                           |
| Sz 125  | 16 12 30.1     | -39 35 40      |                       | Th 44  |

<sup>1</sup>: Spectral types from Hughes et al. (1994) unless otherwise indicated.<sup>2</sup>: Catalog denominations: *Th*: Thé (1962); *KWS97*: Krautter et al. (1997)

Table 12. Classical T Tauri stars in Lupus 4

| Star   | $\alpha(2000)$ | $\delta(2000)$ | Sp. type <sup>1</sup> | Other names <sup>2</sup>            |
|--------|----------------|----------------|-----------------------|-------------------------------------|
| Sz 126 | 15 57 24.1     | -42 39 56      | K7-M0                 | -                                   |
| Sz 127 | 15 57 30.4     | -42 10 28      | M5                    | -                                   |
| Sz 128 | 15 58 07.4     | -41 51 48      | M1.5                  | -                                   |
| Sz 129 | 15 59 16.5     | -41 57 09      | K7-M0                 | Hen 3-1125, Wray 15-1400, SS73 49   |
| Sz 130 | 16 00 31.1     | -41 43 40      | M1.5                  | -                                   |
| MY Lup | 16 00 44.3     | -41 55 31      | K0                    | IRAS 15573-4147, F 403              |
| Sz 131 | 16 00 49.5     | -41 30 08      | M2                    | -                                   |
| Sz 133 | 16 03 29.5     | -41 40 05      | K2                    | -                                   |
| Sz 134 | 16 09 12.2     | -41 40 25      | M1                    | Hen 3-1146, Wray 15-1423            |
| Sz 135 | 16 31 58.3     | -44 31 18      |                       | -                                   |
| Sz 136 | 16 33 04.5     | -44 57 17      |                       | -                                   |
| Sz 137 | 16 33 12.1     | -44 56 14      |                       | -                                   |
| Sz 138 | 16 35 12.2     | -44 58 25      |                       | -                                   |
| Sz 139 | 16 36 10.9     | -44 46 09      |                       | HD 328402, Wray 15-1316, Hen 3-1221 |
| Sz 140 | 16 37 45.7     | -44 54 17      |                       | -                                   |

<sup>1</sup>: Spectral types from Hughes et al. (1994).

<sup>2</sup>: Catalog denominations: *KWS97*: Krautter et al. (1997)

mass function. The very complete census provided by Spitzer also supports a decline in the number of stars with later spectral types. Although Merín et al. (2008) do not provide estimates of individual masses or spectral types, the luminosity function that they derive has a sharp peak at  $L \sim 0.15 L_{\odot}$ , consistent with the peak near M6 found by previous studies. Follow-up spectroscopy of the new members revealed by Spitzer will no doubt help in resolving this matter, once reliable spectral types for the new candidate members have been determined. It may be noted that the fact that these new members are selected on the basis of their infrared excess in the Spitzer bands does not seem to introduce an important incompleteness at low masses, as shown by the small numbers of cool ( $T_{\text{eff}} < 3000$  K) candidate members identified by Comerón et al. (2008, in prep.) on the basis of a fit of their visible/near infrared colors to model photospheres, without making use of any specific youth signature.

The precise shape of the IMF in each region depends on the adopted set of evolutionary tracks, as illustrated by Hughes et al. (1994) by using two state-of-the-art sets of tracks at the time of their study. At the lowest stellar masses the determination of the IMF is little affected by the assumed distance or age, since objects of a given mass evolve at nearly constant temperature and thus the mass is fairly well constrained by the spectral type alone. Therefore, the conclusions on IMF differences among aggregates can be considered as robust, despite considerable advancements in the evolutionary tracks in the decade elapsed since Hughes et al.'s (1994) work.

## 6.2. Ages

The absolute derivation of ages suffers from uncertainties due to possible variability, the adopted distance, and the bolometric correction. As discussed by Hughes et al. (1994), the latter alone introduces an uncertainty of 0.1 dex in  $\log L$ , implying an uncertainty of  $\sim 0.15$  dex in  $\log(\text{Age})$ . The uncertainties in distances discussed in Section 3. are

a larger source of error, as the derived luminosities increase by  $\Delta \log L = 0.25$  if the assumed distance is increased from 150 pc to 200 pc, and the corresponding derived age is decreased by a factor of  $\sim 2$  for a star of  $0.1 M_{\odot}$  of 3 Myr age. Since it is likely that the distances to each of the clouds are significantly different, as discussed in Section 3., it is not currently possible to reliably establish the existence of possible differences among the ages of the stellar populations of each cloud based on the comparison to evolutionary tracks only.

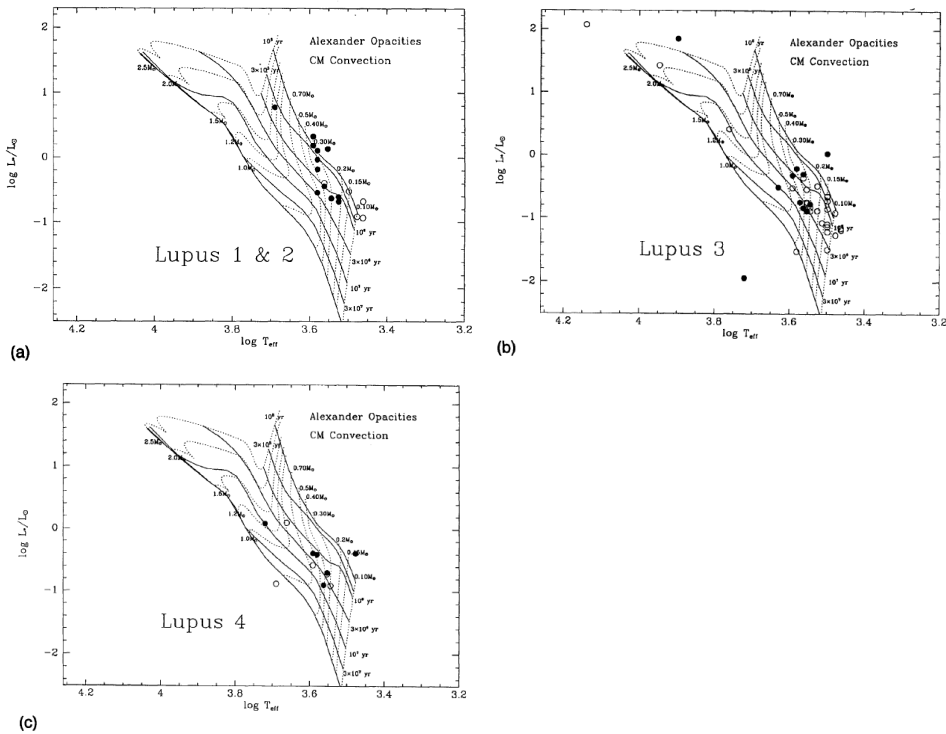


Figure 10. Location of the classical T Tauri stars classified by Hughes et al. (1994) in the temperature-luminosity diagram, compared to theoretical pre-main sequence evolutionary tracks by D’Antona & Mazzitelli (1994). The main caveat when comparing the diagrams for the different regions is that a common distance of 140 pc has been adopted for all of them, which may cause non-real shifts of the data points in the vertical direction. Note that the tracks run nearly vertical at the lowest masses, thus being largely insensitive to an inaccurate distance choice, although their position do change among different sets of evolutionary models. The labels at the top right of each diagram summarize the treatment of interior opacities and convection in the models.

Assuming a distance of 150 pc and adopting the evolutionary tracks of D’Antona & Mazzitelli (1994), Hughes et al. (1994) derived ages formally lying in the range  $4.25 < \log(\text{Age}[\text{yr}]) < 7.25$ , with a peak near 3.2 Myr (see Figure 10, as well as Figure 6 in that paper). The lower limit is particularly unreliable given the large uncertainties of evolutionary models at such early stages (e.g. Baraffe et al. 2002), and the value of the peak is highly dependent on the assumed distance as explained in the previous paragraph, as well as on the adopted models. On the other hand, adopting a distance of

200 pc for their sample in Lupus 3, using their revised spectral type determination, and using the evolutionary tracks of Baraffe et al. (1998), Comerón et al. (2003) derive an age of 1-1.5 Myr for most of their observed members.

With the caveats due to the possible distance differences among clouds, the comparison among the temperature-luminosity diagrams of different clouds hints at Lupus 1 and 2 being younger than Lupus 3 and 4, an interpretation supported by the absence of  $\text{NH}_3$  cores in Lupus 3 and 4. Independent support for a younger age of Lupus 1 has been recently provided by the larger fraction of Class I sources found by Spitzer as compared to the Lupus 3 and 4 clouds (see Merín et al 2008, and Section 6.4.). Similarly, it may be noticed by inspecting Table 5 that despite its conspicuous stellar aggregate Lupus 3 is not particularly rich in protostellar candidates, having a number similar to that of Lupus 5 and Lupus VI where no CTTS have been identified thus far. This may indicate that these two clouds are at the earliest stages of producing stars, while Lupus 3 is more mature in this regard. We also note that the analysis of the Spitzer results (Merín et al. 2008) has revealed a dense, starless core in Lupus 4 where star formation seems likely to proceed in the future, perhaps resulting into a final stellar population in Lupus 4 composed of two distinct bursts separated in time.

Age differences have been tentatively interpreted by some authors in terms of the global star formation history of the region and large-scale agents triggering it. Thus, Tachihara et al. (1996) explained the relative youth of Lupus 1 and 2 as resulting from the recent passage of a shock associated with the expanding Upper Scorpius shell (see Section 2.) across the cloud.

Some peculiar objects have positions in the temperature-luminosity diagram well outside those corresponding to the age ranges given above. Th 28 (Section 7.5.) falls below the main sequence, and Graham & Chen (1994) derive an age of 30 Myr for HH 55 (Section 7.4.) if its position in the temperature-luminosity diagram is taken at face value. A similar conclusion is reached for Par-Lup3-4 (Section 7.6.; Comerón et al. 2003). Alternative explanations for the peculiar position of these objects in such diagrams that do not invoke anomalously old ages have been proposed, and we present them later in the corresponding Sections.

### 6.3. Circumstellar Disks and Envelopes

A first search for cold dust around a sample of 32 optically-selected classical T Tauri members of Lupus 2 and 3 was carried out by Nürnberger et al. (1997). The dust is optically thin at the selected wavelength of 1.3 mm, thus permitting the derivation of masses. Dust emission was detected around 12 of the 32 objects, down to sensitivity limits corresponding to  $M_{\text{dust+gas}} \simeq 5 \times 10^{-3} M_{\odot}$  (to be compared to typical gas+dust masses of  $\sim 3\%$  of the mass of the central object for young CTTS less massive than  $0.7 M_{\odot}$ ). The fraction of objects with dusty envelopes is similar in Taurus-Auriga, Chamaeleon I, and Ophiuchus, also discussed by Nürnberger et al. (1997). A correlation between the emitting mass of dust and the age is found, with no emission detected for any of the objects with an estimated age greater than 3 Myr.

More recent observations of five classical T Tauri stars in Lupus (HT Lup, GW Lup, IM Lup, RU Lup, and HK Lup), probing cold dust at 1.4 mm and 3.3 mm, have been presented by Lommen et al. (2007). All sources except for GW Lup are spatially resolved in these interferometric observations, with disk sizes around 100 AU. The millimeter emission from these disks is confirmed to be optically thin, and disk masses in the 0.019 - 0.033  $M_{\odot}$  range are derived. Evidence is found from the dust opacity

index  $\beta$  (where  $\kappa_\nu \propto \nu^\beta$ ) for grain growth to millimeter sizes and above in the outer regions of the disks. This provides observational support to the theoretical prediction that grain growth in circumstellar disks is a fast process, as predicted by dust coagulation modeling (Dullemond & Dominik 2005).

Merín et al. (2007) have recently reported on SST-Lup3-1, a very low mass star near the brown dwarf boundary in Lupus 3, whose Spitzer IRS spectrum shows strong and highly structured silicate features, indicative of crystalline silicates. The wide wavelength coverage between 5  $\mu\text{m}$  and 35  $\mu\text{m}$  provided by the Spitzer spectrum allows the simultaneous analysis of the silicate features at 10 and 20  $\mu\text{m}$ , which are formed in environments of different temperature, and thus provide spatial information on the dust conditions in different regions of the disk. The analysis of the results provides evidence of rapid dust growth and settling towards the disk midplane. At the same time, the inferred presence of a high fraction of crystalline silicates at large distances from the central object implies either efficient radial mixing, or the existence of mechanisms able to produce annealing of amorphous silicate grains in those regions.

A search for gas in disks in Lupus carried out by van Kempen et al. (2007) using transitions of CO isotopes has confirmed that CO is a poor tracer of gas, probably being either photodissociated or depleted in grains (e.g. Thi et al. 2001), as found in other disks. The only source unambiguously detected out of 21 observed is IM Lup, probably the star possessing the largest and most massive disk in the Lupus region, for which van Kempen et al. (2007) find an outer radius of 400-700 AU. Its CO line profiles are double-peaked, indicative of rotation. The directly derived gas mass is estimated to be  $2 \times 10^{-4} M_\odot$ , over two orders of magnitude below the expected mass from the millimeter continuum observations of Lommen et al. (2007) if a typical interstellar gas-to-dust ratio of 100 is assumed, supporting the notion of strong dissociation or depletion in grains.

Most of the statistical information available on the presence and evolution of disks around young stars in Lupus and other star forming regions comes from the surveys performed by Spitzer. The results on Lupus have been synthesized by Merín et al. (2008), who conclude that the fraction of objects possessing circumstellar disks amounts to 70% - 80%. Their spectral energy distributions suggest that 20% of these are in turn optically thick, flared disks. A wide variety is found in the spectral energy distributions of objects surrounded by disks, both in terms of the shortest wavelength where circumstellar emission begins to dominate and in the spectral index characterizing the slope at long wavelengths. This variety testifies to a broad range of disk structures and inner hole sizes, favoring the scenario of inside-out clearing of circumstellar disks and the existence of very substantial disk evolution in the first few million years of the life of young stellar objects.

#### 6.4. The Lowest-mass Members

As noted above Lupus 3 is the richest aggregate in the region, containing nearly half of the CTTS identified in the Lupus clouds (Table 11). In turn, more than half of the Lupus 3 members are found in the  $0.3 \times 0.3 \text{ pc}^2$  area surrounding the HR 5999 and HR 6000 pair (Nakajima et al. 2000), implying a member density of  $\sim 500$  members per cubic parsec, closer to the stellar density of the Trapezium cluster than to sparse aggregates like the Taurus clouds. This richness has made the center of Lupus 3 (Figures 3 and 11) a preferred target for deep searches of the lowest mass members. Nakajima et al. (2000) identified 10 faint possible members in their near-infrared *JHK* survey of a

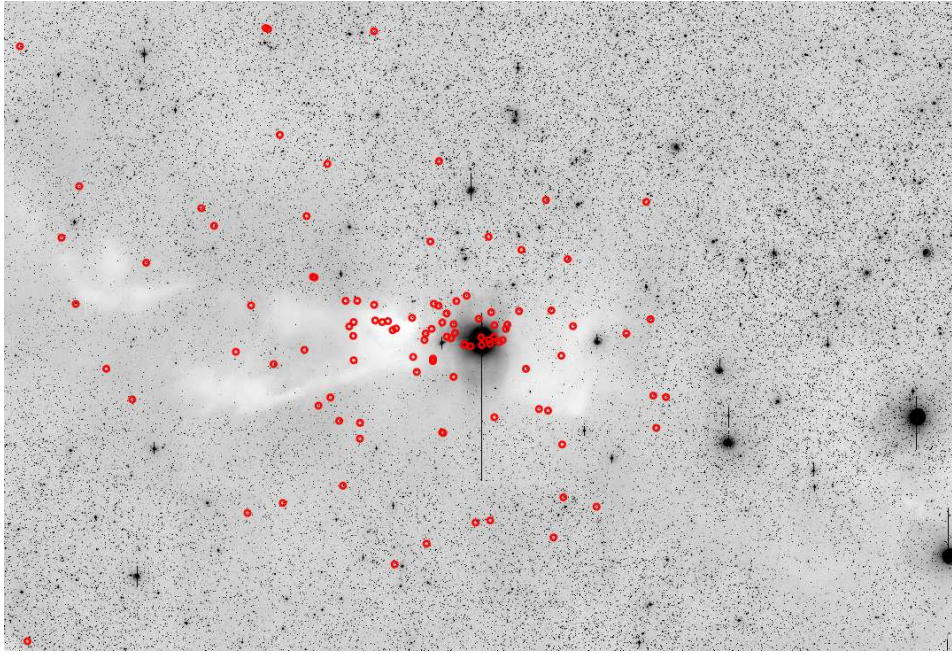


Figure 11. The central region of the Lupus 3 cloud, containing the bright stars HR 5999 and HR 6000 near the center of the field. Red circles indicate the positions of all the candidate members selected in Spitzer observations of the region, plus other known members not fulfilling the Spitzer infrared excess criteria but previously identified using other techniques, according to the compilation of Merín et al. (2008). This compilation provides the most complete census of members of Lupus 3 available to date. The clustering towards HR 5999 and HR 6000 is clearly seen. The image was taken through the  $R$  filter with the Wide Field Imager at the MPI-ESO 2.2m telescope on La Silla. From a still unpublished survey by the author in support of the Spitzer 'Cores to Disks' Legacy program.

$7' \times 11'$  area East of HR 5999/6000 on the basis of their  $K$ -band excess, all of which are brown dwarf candidates for their assumed distance (150 pc) and age (1 Myr). An additional 11 sources are undetected at  $J$  and have very red  $H - K$  colors unlikely to be due to extinction alone. The membership of most of these objects has been further confirmed by the detection of excess at longer infrared wavelengths by Spitzer. We list in Table 13 the objects appearing in Nakajima et al. (2000) whose membership is supported by the Spitzer observations presented by Merín et al. (2008).

Their results suggest that the preference towards small masses at Lupus extends down into the substellar regime, given the higher abundance of brown dwarfs in Lupus with respect to Taurus by a factor of 4:1 when candidates are selected based on the same selection criteria. The pre-main sequence stars tend to concentrate towards the position of  $C^{18}O$  and  $^{13}CO$  cores (Tachihara et al. 1996, Hara et al. 1999; see also Sect. 4.), with peak densities in the  $1000-3000 \text{ pc}^{-3}$  range, although the latter are poorly determined due to the small numbers involved and the ill-defined sizes of the concentrations. We note however that Nakajima et al.'s (2000) results concerning the abundance of very low mass members seem to be in contrast with the results of surveys using different techniques for identification that include the same area, such as that of López Martí et

Table 13. Suspected Lupus 3 members from Nakajima et al. (2000) with detected infrared excess in the Spitzer bands

| Name        | $\alpha(2000)$ | $\delta(2000)$ |
|-------------|----------------|----------------|
| 0526.9–5630 | 16 08 28.16    | –39 04 24.6    |
| 0532.1–5616 | 16 08 53.68    | –39 04 09.6    |
| 0536.7–5943 | 16 08 58.27    | –39 07 35.5    |
| 0536.7–5956 | 16 08 58.30    | –39 07 49.4    |
| 0537.4–5653 | 16 08 58.92    | –39 04 46.0    |
| 0540.9–5757 | 16 09 02.44    | –39 05 49.4    |
| 0546.4–5934 | 16 09 07.98    | –39 07 26.4    |
| 0554.9–5651 | 16 09 16.43    | –39 04 43.7    |
| 0558.8–5610 | 16 09 20.30    | –39 04 01.6    |
| 0601.7–5616 | 16 09 23.15    | –39 04 07.4    |
| 0605.1–5606 | 16 09 26.61    | –39 03 57.7    |
| 0605.6–5437 | 16 09 27.08    | –39 02 28.4    |
| 0614.0–5414 | 16 09 35.37    | –39 02 05.4    |
| 0615.6–5616 | 16 09 37.15    | –39 04 06.9    |
| 0615.6–5953 | 16 09 37.19    | –39 07 44.7    |
| 0615.8–5734 | 16 09 37.38    | –39 05 25.7    |
| 0617.7–5641 | 16 09 39.29    | –39 04 31.8    |
| 0619.6–5414 | 16 09 41.08    | –39 02 05.6    |

Table 14. Additional low-mass members of Lupus 3 from Comerón et al. (2003)

| Star       | $\alpha(2000)$ | $\delta(2000)$ | Sp. type |
|------------|----------------|----------------|----------|
| Par-Lup3-1 | 16 08 15.9     | –39 03 07      | M7.5     |
| Par-Lup3-2 | 16 08 35.7     | –39 03 48      | M6       |
| Par-Lup3-3 | 16 08 49.3     | –39 05 38      | M4.5     |
| Par-Lup3-4 | 16 08 51.4     | –39 05 31      | M5       |

al. (2005) outlined in Sect. 6.1. and described in more detail below, or the most recent Spitzer results summarized in that same Section. Such apparent discrepancies emphasize the need for detailed spectroscopic classifications firmly establishing membership at the time of extracting conclusions on the faint end of the luminosity function.

Deep slitless spectroscopy around the  $H\alpha$  line carried out by Comerón et al. (2003) in an area of  $9'.7 \times 5'.1$  centered near HR5999/6000 has identified four new late-type emission-line objects with spectral types between M4.5 and M7.5, listed in Table 14. The latest of these objects, Par-Lup3-1, is almost certainly a brown dwarf, clearly later than the M6-M6.5 spectral type that marks the end of the stellar range in star forming regions of a few million years of age. A mass of  $0.04 M_{\odot}$  is estimated using evolutionary models by Baraffe et al. (1998). The follow-up multiobject spectroscopy carried out by Comerón et al. (2003) has also allowed them to classify the sources already observed by Hughes et al. (1994). Interestingly, a systematic difference of approximately two spectral subclasses is found between both classifications (Table 15), which

Table 15. Comparison between spectral types assigned by Hughes et al. (1994) and Comerón et al. (2003) to members of Lupus 3

| Star   | Sp. type (Hughes et al.) | Sp. type (Comerón et al.) |
|--------|--------------------------|---------------------------|
| Sz 100 | M5                       | M5                        |
| Sz 106 | M0                       | M2.5                      |
| Sz 108 | M1                       | M3 + M6                   |
| Sz 109 | M5.5                     | M6.5                      |
| Sz 110 | M2                       | M4.5                      |
| Sz 112 | M4                       | M6                        |
| Sz 113 | M4                       | M6                        |
| Sz 114 | M4                       | M5.5                      |

Table 16. Possible very low mass members of Lupus 3 with likely H $\alpha$  emission. From López Martí et al. (2005)

| Star                  | $\alpha(2000)$ | $\delta(2000)$ | $I$   | sp. type <sup>1</sup> |
|-----------------------|----------------|----------------|-------|-----------------------|
| Lup 504               | 16 06 47.0     | -39 16 15      | 14.94 | M4                    |
| Lup 604s <sup>2</sup> | 16 08 00.2     | -39 02 59      | 14.36 | M5.5                  |
| Lup 608s              | 16 09 08.5     | -39 03 43      | 14.24 | M5                    |
| Lup 609s              | 16 08 57.8     | -39 02 23      | 14.88 | M5                    |
| Lup 605               | 16 07 14.0     | -38 52 37      | 16.46 | M6.5                  |
| Lup 607 <sup>2</sup>  | 16 08 28.1     | -39 13 09      | 16.10 | M5                    |
| Lup 617               | 16 08 48.2     | -39 09 20      | 15.02 | M6                    |
| Lup 642               | 16 09 01.5     | -39 05 06      | 19.9: | L2                    |
| Lup 648               | 16 09 48.6     | -39 11 17      | 15.28 | M5                    |
| Lup 650               | 16 09 49.8     | -38 49 04      | 17.62 | M4                    |
| Lup 652               | 16 07 09.5     | -38 41 30      | 18.36 | M4.5                  |
| Lup 654               | 16 07 23.4     | -39 05 13      | 17.25 | L1                    |
| Lup 710               | 16 09 17.1     | -39 27 09      | 15.84 | M5                    |
| Lup 713               | 16 07 37.7     | -39 21 38      | 15.66 | M6                    |
| Lup 706 <sup>2</sup>  | 16 08 37.3     | -39 23 10      | 18.27 | L0                    |
| Lup 707 <sup>2</sup>  | 16 08 28.1     | -39 13 09      | 16.09 | M5                    |
| Lup 714               | 16 07 58.9     | -39 24 35      | 14.81 | M5                    |
| Lup 802s              | 16 11 51.2     | -38 51 04      | 15.29 | M4                    |
| Lup 810s              | 16 09 54.6     | -39 12 03      | 14.84 | <M4                   |
| Lup 818s <sup>2</sup> | 16 09 56.3     | -38 59 52      | 15.25 | M6                    |
| Lup 831s              | 16 11 38.6     | -39 08 27      | 15.32 | <M4                   |
| Lup 914               | 16 10 16.1     | -39 37 53      | 15.81 | <M4                   |
| Lup 915               | 16 10 54.1     | -39 40 07      | 14.05 | M4                    |

<sup>1</sup>: Spectral types are estimated from narrow-band imaging

<sup>2</sup>: Also detected with mid-infrared excess by Spitzer (Allen et al. 2007)

is larger than the uncertainty in the classification estimated by Hughes et al. (1994). Comerón et al. (2003) tentatively attribute this to the different spectral ranges where each classification is carried out, the one used by Hughes et al. (1994) being bluer and thus more prone to the effects of veiling. All four new members detected by Comerón et al. (2003) are detected Spitzer (Merín et al. 2008) on the basis of their infrared excess longwards of  $3.6 \mu\text{m}$ , which is moderate for Par-Lup3-1 and 2. In contrast, Par-Lup3-3 and Par-Lup3-4 have strong infrared excesses corresponding to Class I spectral energy distributions; see Sect. 7.6. for a more detailed discussion on the latter object.

The identification of members of Lupus in the studies mentioned above is based on either  $\text{H}\alpha$  emission or near-infrared excess, and may thus be biased against the detection of possible members lacking such signatures of accretion or circumstellar material near the surface of the star. In her analysis of a deep, large-area imaging survey of Lupus 3, López Martí (2003) selects candidate members by a combination of broad- and narrow-band colors that provide a rough spectral type estimate independently of the presence of accretion or warm disk signatures. The former can nevertheless still be suspected from the comparison between the  $R$ -band and  $\text{H}\alpha$  imaging discussed in that study. Although spectroscopic confirmation of the new candidate members has not been presented yet, the study demonstrates its ability to probe well into the substellar regime, probably down to L spectral types (Kirkpatrick et al. 1999). A few objects possibly having early L types are indeed presented by López Martí et al. (2005); Table 16 lists the best new candidate members identified in that work whose membership in Lupus 3 is reinforced by the presence of  $\text{H}\alpha$  emission. Indeed, narrow-band imaging in  $\text{H}\alpha$  shows that emission is common around these objects with no apparent decrease towards lower luminosities, in line with recent discoveries of strong  $\text{H}\alpha$  emitters with late spectral M types (e.g. Barrado y Navascués 2004a).

An alternative approach to the identification of young aggregate members is based on the detection of infrared excesses caused by circumstellar dust. Very low mass young stellar objects rarely display near-infrared excesses at wavelengths as short as  $2 \mu\text{m}$ , probably due to the absence of sufficient amounts of dust hot enough to contribute to the emission at that wavelength (Comerón et al. 2000). However, colder dust produces noticeable effects in the spectral energy distribution at longer wavelengths. The recent availability of sensitive large-area surveys at wavelengths between  $3 \mu\text{m}$  and  $70 \mu\text{m}$  covering the densest parts of the Lupus complex, carried out with Spitzer, has made possible the detection of large numbers of candidate low mass objects and the determination of the spectral energy distribution of already known members over a much broader wavelength range. Some of the implications of these new results have been presented in previous Sections.

Observations of Lupus 1, 3 and 4 reported by Chapman et al. (2007) using the MIPS camera onboard Spitzer, which operates between  $24$  and  $170 \mu\text{m}$ , have revealed many new candidate members of these clouds by combining near- and mid-infrared color-color selection criteria, showing that a combination of 2MASS and MIPS flux measurements is efficient in separating background galaxies from young stellar objects with infrared excess. A total of 103 candidate YSOs are identified, of which approximately one third of them had been previously identified. In addition, about two thirds of the classical T Tauri stars previously known in the area are identified by these criteria. Most of the objects displaying mid-infrared excesses belong to Class II and III, with an overall fraction of 10-20% Class I sources. Within the small-number statistics, the

fraction of Class I sources seems to be larger in Lupus 1, where 7 out of 17 mid-infrared selected objects are Class I.

Table 17. Additional low-mass members of Lupus 3 from Allen et al. (2007) identified by their mid-infrared excess and spectroscopically confirmed

| Star              | $K_S^1$ | Sp. type |
|-------------------|---------|----------|
| J16073773–3921388 | 12.13   | M5.75    |
| J16080017–3902595 | 11.07   | M5.25    |
| J16081497–3857145 | 13.13   | M4.75    |
| J16083733–3923109 | 13.83   | M7.75    |
| J16085373–3914367 | 12.52   | M5.5     |
| J16085953–3856275 | 12.84   | M8       |

<sup>1</sup>:  $K_S$  magnitude from the 2MASS point source catalog.

Table 18. Possible additional low mass members of Lupus 3 with mid-infrared excess detected by Spitzer. From Allen et al. (2007)

| Star                           | $K_S^1$ |
|--------------------------------|---------|
| J16075475–3915446              | 14.45   |
| J16080175–3912316              | 14.25   |
| J16080618–3912225              | 7.67    |
| J16083010–3922592 <sup>2</sup> |         |
| J16083110–3856000 <sup>2</sup> |         |
| J16084679–3902074 <sup>2</sup> |         |
| J16084747–3905087              | 14.83   |
| J16085324–3914401              | 9.80    |
| J16085529–3848481              | 12.02   |
| J16093418–3915127 <sup>2</sup> |         |
| J16100133–3906449.             | 10.52   |

<sup>1</sup>:  $K_S$  magnitude from the 2MASS point source catalog.

<sup>2</sup>: No entry in the 2MASS point source catalog.

Also using joint IRAC and MIPS data, Allen et al. (2007) identify 19 new low-mass star and brown dwarf members of Lupus 3 based on their 3.6  $\mu\text{m}$  - 8.0  $\mu\text{m}$  excess. In addition, their selection criterion identifies 41 previously known members, of which 3 were reported as likely  $\text{H}\alpha$  emitters by López Martí (2005). Of the newly identified candidate members, 6 were spectroscopically observed in the visible and confirmed as members, with spectral types between M4.75-M8. Those authors also observed 2M1541-3345 near Lupus 1, which was first identified by Jayawardhana & Ivanov (2006) as a brown dwarf, and reclassified as a low-mass star probably older than

most members of Lupus 1. The new members are listed in Tables 17 (spectroscopically confirmed members) and 18 (other candidate members).

Table 19. Candidate low-mass members of Lupus 1 with mid-infrared excess (Allers et al. 2006)

| Star | $\alpha(2000)$ | $\delta(2000)$ | $K_S$ |
|------|----------------|----------------|-------|
| 17   | 15 39 27.3     | -34 48 44      | 15.69 |
| 18   | 15 41 40.8     | -33 45 19      | 13.75 |
| 19   | 15 44 57.9     | -34 23 39      | 12.10 |

Similarly, 3 new members of Lupus 1 identified on the basis of their joint near-infrared and Spitzer ( $3.6 \mu\text{m} - 24 \mu\text{m}$ ) photometry have been identified by Allers et al. (2006). These authors estimate physical parameters from IJHK photometry. The derived masses are very low, well below the brown dwarf limit, and estimated to lie between 6 and 50 Jupiter masses ( $M_{\text{Jup}}$ ). These three objects are listed in Table 19.

All the available Spitzer imaging data obtained on Lupus with IRAC and MIPS have been synthesized by Merín et al. (2008), who have compiled the most complete census of members of Lupus 1, 3, and 4 available to date. The additional members not listed in any of the previous tables are presented in Tables 20, 21, and 22.

Table 20. Remaining candidate members of Lupus 1 identified with Spitzer (Merín et al. 2008)

| Object                  | $\alpha(2000)$ | $\delta(2000)$ | Class <sup>1</sup> |
|-------------------------|----------------|----------------|--------------------|
| SSTc2d J153803.1-331358 | 15 38 03.10    | -33 13 57.7    | III                |
| SSTc2d J153848.2-344041 | 15 38 48.36    | -34 40 38.2    | I                  |
| SSTc2d J154214.6-341026 | 15 42 14.57    | -34 10 25.8    | I                  |
| SSTc2d J154240.3-341343 | 15 42 40.32    | -34 13 43.0    | III                |
| SSTc2d J154301.3-340915 | 15 43 01.29    | -34 09 15.4    | F                  |
| SSTc2d J154302.3-344406 | 15 43 02.29    | -34 44 06.2    | F                  |
| SSTc2d J154506.3-341738 | 15 45 06.34    | -34 17 38.2    | F                  |
| SSTc2d J154508.9-341734 | 15 45 08.88    | -34 17 33.7    | II                 |
| SSTc2d J154518.5-342125 | 15 45 18.53    | -34 21 24.8    | II                 |

<sup>1</sup>: Spectral energy distribution class according to the classification scheme of Lada & Wilking (1984), extended by Greene et al. (1994).

## 6.5. Star Formation Efficiency

The star formation efficiency, defined as  $SFE = M_{\text{stars}}/M_{\text{stars+gas}}$  was first estimated by Tachihara et al. (1996) by comparing their CO observations with the known stellar population of each cloud. They derived  $SFE \simeq 0.04$  for Lupus 3, but the preference of the Lupus clouds towards forming very low-mass objects (Section 6.1.) makes this estimate very dependent on the completeness of the census at the lowest masses, as well

Table 21. Remaining candidate members of Lupus 3 identified with Spitzer (Merín et al. 2008)

| Object                  | $\alpha(2000)$ | $\delta(2000)$ | Class <sup>1</sup> |
|-------------------------|----------------|----------------|--------------------|
| SSTc2d J160703.9–391112 | 16 07 03.85    | –39 11 11.6    | F                  |
| SSTc2d J160708.6–391407 | 16 07 08.57    | –39 14 07.7    | F                  |
| SSTc2d J160708.6–394723 | 16 07 08.64    | –39 47 22.7    | II                 |
| SSTc2d J160754.1–392046 | 16 07 54.09    | –39 20 46.2    | III                |
| SSTc2d J160755.3–390718 | 16 07 55.29    | –39 07 17.8    | III                |
| SSTc2d J160803.0–385229 | 16 08 03.02    | –38 52 29.3    | III                |
| SSTc2d J160830.7–382827 | 16 08 30.70    | –38 28 26.8    | II                 |
| SSTc2d J160901.4–392512 | 16 09 01.40    | –39 25 11.9    | II                 |
| SSTc2d J160927.0–383628 | 16 09 26.98    | –38 36 27.6    | II                 |
| SSTc2d J160934.1–391342 | 16 09 34.11    | –39 13 42.1    | III                |
| SSTc2d J161000.1–385401 | 16 10 00.11    | –38 54 01.1    | III                |
| SSTc2d J161013.1–384617 | 16 10 13.06    | –38 46 16.8    | F                  |
| SSTc2d J161018.6–383613 | 16 10 18.56    | –38 36 13.0    | II                 |
| SSTc2d J161019.8–383607 | 16 10 19.84    | –38 36 06.8    | II                 |
| SSTc2d J161027.4–390230 | 16 10 27.43    | –39 02 30.2    | F                  |
| SSTc2d J161029.6–392215 | 16 10 29.57    | –39 22 14.7    | II                 |
| SSTc2d J161032.6–374615 | 16 10 32.59    | –37 46 14.9    | III                |
| SSTc2d J161034.5–381450 | 16 10 34.51    | –38 14 50.3    | III                |
| SSTc2d J161035.0–390655 | 16 10 34.97    | –39 06 54.6    | III                |
| SSTc2d J161045.4–385455 | 16 10 45.38    | –38 54 54.9    | II                 |
| SSTc2d J161118.7–385824 | 16 11 18.69    | –38 58 23.6    | III                |
| SSTc2d J161126.0–391123 | 16 11 25.98    | –39 11 23.2    | III                |
| SSTc2d J161131.9–381110 | 16 11 31.93    | –38 11 10.4    | III                |
| SSTc2d J161144.9–383245 | 16 11 44.86    | –38 32 44.7    | III                |
| SSTc2d J161148.7–381758 | 16 11 48.67    | –38 17 58.3    | II                 |
| SSTc2d J161159.8–382339 | 16 11 59.81    | –38 23 38.5    | II                 |
| SSTc2d J161200.1–385557 | 16 12 00.06    | –38 55 56.9    | III                |
| SSTc2d J161204.5–380959 | 16 12 04.48    | –38 09 59.0    | F                  |
| SSTc2d J161211.2–383220 | 16 12 11.22    | –38 32 19.8    | II                 |
| SSTc2d J161218.5–393418 | 16 12 18.47    | –39 34 18.3    | I                  |
| SSTc2d J161219.6–383742 | 16 12 19.60    | –38 37 42.2    | III                |
| SSTc2d J161222.7–371328 | 16 12 22.73    | –37 13 27.6    | II                 |
| SSTc2d J161243.8–381503 | 16 12 43.75    | –38 15 03.3    | II                 |
| SSTc2d J161251.7–384216 | 16 12 51.72    | –38 42 16.0    | III                |
| SSTc2d J161256.0–375643 | 16 12 55.96    | –37 56 43.8    | III                |
| SSTc2d J161341.0–383724 | 16 13 40.95    | –38 37 23.7    | III                |
| SSTc2d J161344.1–373646 | 16 13 44.11    | –37 36 46.4    | II                 |

<sup>1</sup>: Spectral energy distribution class according to the classification scheme of Lada & Wilking (1984), extended by Greene et al. (1994).

as of the sensitivity to the low column density outskirts of the cloud where much of its molecular mass can be located. For the other clouds, Tachihara et al. (1996) estimated much lower efficiencies, always below 0.01. Such low overall star formation efficiency might be explained by the strong and unshielded UV flux from the Scorpius-Centaurus association (Tachihara et al. 2001), a cause that has been invoked to explain a similarly

Table 22. Remaining candidate members of Lupus 4 identified with Spitzer (Merín et al. 2008)

| Object                  | $\alpha(2000)$ | $\delta(2000)$ | Class <sup>1</sup> |
|-------------------------|----------------|----------------|--------------------|
| SSTc2d J155925.2–423507 | 15 59 25.24    | –42 35 07.1    | II                 |
| SSTc2d J155945.3–415457 | 15 59 45.28    | –41 54 57.2    | II                 |
| SSTc2d J160000.6–422158 | 16 00 00.62    | –42 21 57.5    | II                 |
| SSTc2d J160002.4–422216 | 16 00 02.37    | –42 22 15.5    | II                 |
| SSTc2d J160007.4–414949 | 16 00 07.43    | –41 49 48.9    | II                 |
| SSTc2d J160026.1–415356 | 16 00 26.13    | –41 53 55.6    | II                 |
| SSTc2d J160034.4–422540 | 16 00 34.39    | –42 25 39.5    | II                 |
| SSTc2d J160111.6–413730 | 16 01 11.55    | –41 37 30.1    | III                |
| SSTc2d J160115.6–415235 | 16 01 15.55    | –41 52 35.3    | F                  |
| SSTc2d J160129.7–420804 | 16 01 29.69    | –42 08 03.6    | III                |
| SSTc2d J160143.3–413606 | 16 01 43.28    | –41 36 05.7    | III                |
| SSTc2d J160157.0–414244 | 16 01 57.04    | –41 42 43.9    | III                |
| SSTc2d J160221.6–414054 | 16 02 21.61    | –41 40 53.7    | I                  |
| SSTc2d J160229.9–415111 | 16 02 29.91    | –41 51 11.1    | III                |

<sup>1</sup>: Spectral energy distribution class according to the classification scheme of Lada & Wilking (1984), extended by Greene et al. (1994).

low efficiency in the Ophiuchus North region, where  $SFE$  is estimated to be no higher than 0.003 (Nozawa et al. 1991).

The problem has been reexamined by Merín et al. (2008) using the more complete stellar and substellar census provided by Spitzer and extinction maps also derived from Spitzer observations. These authors stress the uncertainties introduced by the determination of the mass in the molecular gas, and derive star formation efficiencies ranging from below  $\sim 1\%$  when all the molecular gas is considered, to above 10% in Lupus 3 when only the mass in dense cores is taken into account. They also find that the star formation efficiency scales roughly linearly with the core mass, in that the most massive cores appear to be more efficient at forming stars.

## 6.6. The Weak-line T Tauri Stellar Population

Like in other star forming regions, the availability of the ROSAT All-Sky Survey has dramatically increased the number of known members in the general region of the Lupus clouds by revealing a population of low-mass stars emitting in X-rays probably due to coronal heating (as is also the case in older late-type stars; Wichmann et al. 1997b) and weak or no  $H\alpha$  emission, the weak-line T Tauri stars. The oldest WTTS may be representatives of the post-TTS phase proposed by Herbig (1978), characterized by relatively strong X-ray emission at an evolutionary stage at which all other tracers of youth have already disappeared.

The ROSAT observations in Lupus reported by Krautter et al. (1997) reveal 136 objects, including both already known CTTS and new WTTS. The pre-main sequence nature of these objects is confirmed by the presence of lithium. The most distinctive characteristic of the new WTTS population is that unlike CTTS they do not concentrate towards the main clouds, but are found widespread across the entire region (Figure 12).

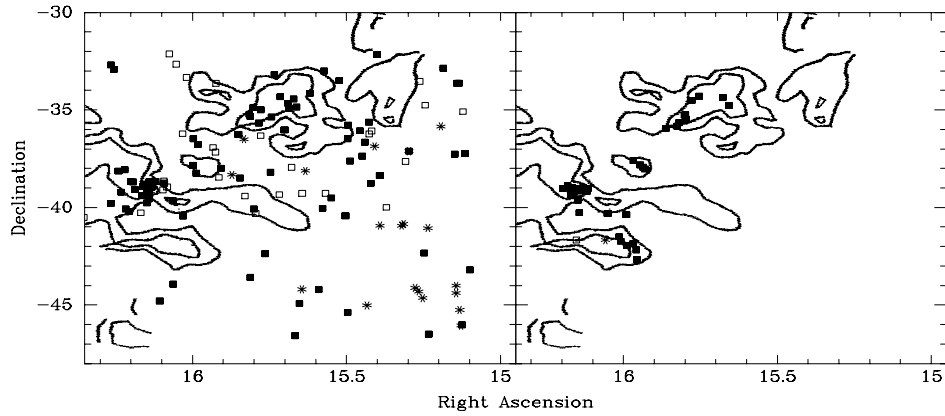


Figure 12. Distribution of T Tauri stars (both classical and weak-line) in the proximities of Lupus 1, 2, and 3. The right panel shows the positions of classical T Tauri stars selected from their properties in the visible, and the left panel the positions of sources detected in the ROSAT All-Sky Survey. The different symbols indicate ages (younger than 5 Myr for filled squares, between 5 and 10 Myr for open squares, and older than 10 Myr for asterisks). The contours indicate the large-scale distribution of  $^{12}\text{CO}$ . From Wichmann et al. (1997b).

Based on approximate completeness corrections, Krautter et al. (1997) estimate a total of  $\sim 650$  WTTS members in the region, outnumbering the population of CTTS by a factor  $> 10$  and still being as numerous as CTTS in the dense clouds.

The weak correlation between the position of the WTTS and that of the denser smaller clouds that emerges from the analysis of ROSAT data for the nearby star forming regions (e.g. Wichmann 1996) has led several authors to wonder whether these stars formed near their current locations in now-dissipated cloudlets, or rather they were formed in the observed clouds with peculiar velocities that have brought them outside (Feigelson 1996). Either scenario requires the WTTS to be older than CTTS. Wichmann et al. (1997b) find young WTTS at distances of the clouds that imply relatively large velocities,  $> 3 \text{ km s}^{-1}$ , and that may be the result of companion ejection in close encounters of binary systems (Sterzik & Durisen 1995). However, given the ages derived by Wichmann et al. (1997b) a smaller velocity dispersion of only  $1 \text{ km s}^{-1}$  suffices to explain the spatial dispersion of the WTTS population without need for in-situ formation in cloudlets. A different conclusion is reached by Tachihara et al. (2001), on the basis of the statistics of star-to-cloud distances that seems to favor the scenario of formation in clouds rapidly evaporating under the influence of Scorpius-Centaurus massive stars.

A further difficulty in observationally addressing the problem of the origin of WTTS stars in Lupus is due to the possibility that two different populations coexist. Wichmann et al. (1997a) have shown that most of the ROSAT WTTS population in Lupus is clearly associated with the Gould Belt rather than to the Lupus clouds themselves, and that it extends beyond the boundaries of the Lupus clouds. This population is likely to be a part of a generic Gould Belt population that could be traced out along most of its great circle with ROSAT data by Guillout et al. (1998), and its distance in the direction of Lupus is similar or slightly smaller than that of the clouds (Wichmann et al. 1999). At the age of the Gould Belt (60 Myr; Pöppel 1997, or perhaps as young as

30 Myr according to Comerón 1999) WTTS should still appear as pre-main sequence objects. This has been confirmed for 46 members by Wichmann et al. (1997b), who detected lithium in the spectrum of 43 off-cloud WTTS members. Whereas the relationship of the WTTS to the Gould Belt is clearly established, their relationship to the Lupus clouds is nevertheless less clear. Wichmann et al. (1997b) found that the WTTS projected against the Lupus clouds are on the average younger than the rest, with a typical age of  $\sim 7$  Myr, although not as young as the CTTS population discussed in Section 6.2. Furthermore, the preference towards low masses that characterizes CTTS in the Lupus clouds (Section 6.1.) does not seem to exist among the WTTS. The distance of the overall WTTS population is similar to, or perhaps slightly less than, the distance to the clouds (Wichmann et al. 1999), and positive velocities confirm the association with the expanding Gould Belt. Similar results obtained by Covino et al. (1997) in Chamaeleon I, where similar ages for the WTTS and CTTS populations are found under the assumption that both are located at the same distance.

Tachihara et al. (2001) have suggested that WTTS west of Lupus, being older and outside the Upper Scorpius bubble, may be related to the Upper Centaurus group, whereas the origin of the on-cloud population including the CTTS could have been triggered by the Upper Scorpius bubble, estimated to be 1.5 Myr old (de Geus 1992). Such scenario is consistent with the young ages of stars in Lupus 1 and 2 estimated by Hughes et al. (1994), and also with those of Lupus 3 if the longer distance proposed by Comerón et al. (2003) is adopted.

A sensitive search for infrared excesses around weak-line T Tauri stars carried out by Padgett et al. (2006) using MIPS at the Spitzer Space Observatory has found them to be very rare, being present in only 5 out of a sample of 83 targets observed, including 37 in Lupus. This supports the prevailing interpretation of weak-line T Tauri stars as young stellar objects that have lost their disks. The majority of targets in the study of Padgett et al. (2006) are located a few degrees away from the main clouds. A complementary study by Cieza et al. (2007), using observations with both IRAC and MIPS onboard Spitzer, has focused on the WTTS on and around the star forming clouds. Their findings are significantly different from those of Padgett et al. (2006) in yielding a much larger fraction of WTTS with infrared excess, up to 20% of their sample in the IRAC bands ( $< 8 \mu\text{m}$ ). The authors interpret the results as indicating an actual differences between the ages of the on-cloud and off-cloud WTTS populations, with the WTTS projected on the clouds representing the youngest part of the age distribution. The coexistence and coevality of the youngest WTTS with CTTS argues for a fast dissipation timescale of disks on the average, but also for large differences from one object to another in this regard. In particular, some of the youngest WTTS do not display infrared signatures of a circumstellar disk, implying that disk dissipation can take place in a time span as short as 1 Myr.

One of the WTTS in the outskirts of Lupus 1, MO Lup, has been recently found to be a hierarchical triple system (Esposito et al. 2007). The main component of the system is a double-lined K7 spectroscopic binary with a 11.95 days period and a photometric variability period of 4.41 days, probably due to star spots. Radial velocity monitoring by those authors strongly suggest the existence of a third body with a mass not much above  $0.2 M_{\odot}$  with an orbital period of several years, most probably  $\sim 6.2$  years. Another interesting weak-line T Tauri star that has received recent attention is MN Lup, near Lupus 3, which Strassmeier et al. (2005) find to be a very fast rotator with a rotation period of only 10.5 hours. Those authors use high resolution spectroscopy to

produce Doppler imaging of the stellar surface and resolve what appear to be accretion shocks, suggesting that the very fast rotation (only three times above the break-up rotational velocity) may be due to the spin-up of the star by infalling gas.

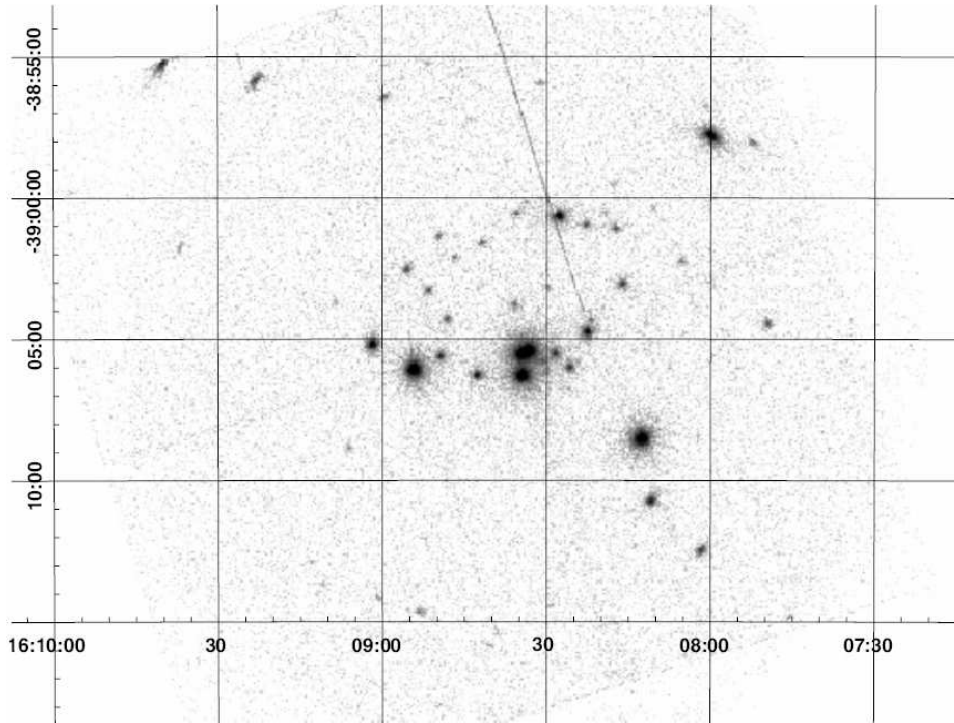


Figure 13. X-ray image of the region around the center of the Lupus 3 cloud obtained by the XMM-Newton satellite. The photon energy range is between 0.5 and 4.5 keV. The two bright sources at the center are HR 5999 and HR 6000. The image combines 6-hour exposures taken with the EPIC instrument MOS1, MOS2, and PN cameras. From Gondoin (2006).

### 6.7. X-ray Emission in Lupus 3

In addition to the all-sky, moderate sensitivity X-ray observations carried out by the ROSAT satellite in the 1990s, which led to the discovery of the weak-line T Tauri population described in Section 6.6., more sensitive pointed observations of Lupus 3 have been carried out both with ROSAT and, more recently, with XMM-Newton (Figure 13). The latter have been described by Gondoin (2006), who reports the discovery of 102 sources in a  $30'$  diameter field approximately centered on HR 5999/6000, and presents an analysis of the 24 sources that can be associated with previously known members. This largely increases the number of X-ray emitters identified in the region, where only 6 had been detected by previous observations. Besides, upper limits are given for 7 additional stars.

A comparison with the results of observations at other wavelengths shows that all the stars more massive than  $\simeq 0.5 M_{\odot}$  are detected by these observations. The X-ray to bolometric luminosity ratios derived are in the range typically found for very young low-mass stars, from  $-4.3 < \log(L_X/L_{\text{bol}}) < -3$  (see Table 23), the upper limit

Table 23. X-ray emission properties of Lupus 3 members with optical counterparts. From Gondoin (2006)

| Star                    | $L_X$ ( $10^{28}$ ) erg s $^{-1}$ <sup>1</sup> | $\log(L_X/L_{bol})$ |
|-------------------------|--|---------------------|
| Sz 94                   | $8.3 \pm 0.7$                                  | -3.51               |
| Sz 95                   | $13.0 \pm 1.6$                                 | -3.72               |
| RX J1608.0-3857         | $128.5 \pm 3.2$                                | -3.06               |
| RX J1608.2-3910         | $26.6 \pm 1.3$                                 | -3.60               |
| Sz 96                   | $278.0 \pm 4.0$                                | -2.60               |
| Par-Lup3-1 <sup>2</sup> | $7.9 \pm 0.6$                                  | -3.39               |
| Sz 98                   | $43.5 \pm 1.8$                                 | -3.74               |
| RX J1608.5-3900B        | $6.6 \pm 1.1$                                  | -3.54               |
| Sz 100                  | $18.5 \pm 1.2$                                 | -3.40               |
| RX J1608.5-3900A        | $51.9 \pm 1.7$                                 | -3.01               |
| Sz 101                  | $20.9 \pm 1.3$                                 | -3.54               |
| Sz 102                  | $3.8 \pm 0.7$                                  | -3.07               |
| Par-Lup3-2              | $4.3 \pm 0.5$                                  | -4.22               |
| Sz 107                  | $4.0 \pm 0.5$                                  | -3.82               |
| Sz 108 <sup>3</sup>     | $17.8 \pm 0.9$                                 | -3.96               |
| Sz 109                  | $7.0 \pm 0.7$                                  | -3.59               |
| Par-Lup3-3              | 27.72.2  | -3.96               |
| Sz 110                  | $14.6 \pm 1.4$                                 | -3.66               |
| RX J1608.9-3905         | $318.2 \pm 5.7$                                | -2.96               |
| Sz 112                  | $18.3 \pm 1.4$                                 | -3.47               |
| Sz 114                  | $90.4 \pm 2.9$                                 | -2.97               |
| Sz 115                  | $3.1 \pm 0.5$                                  | -4.0                |
| Sz 97                   | < 3.8  | < - - 4.10          |
| Sz 99                   | < 4.7  | < - - 3.82          |
| Sz 103                  | < 2.7  | < - - 3.92          |
| Sz 104                  | < 2.7  | < - - 3.85          |
| Sz 106                  | < 3.5  | < - - 3.52          |
| Sz 113                  | < 4.7  | < - - 3.39          |
| Par-Lup3-4              | < 13.8   | < - - 2.2           |

<sup>1</sup>: X-ray luminosity assuming a distance of 140 pc. X-ray luminosities need to be multiplied by 2 if the distance of 200 pc to Lupus recommended in this paper is adopted instead

<sup>2</sup>: This includes the possible contribution of the companion candidate reported by Comerón et al. (2003), although according to these authors the companion is probably a background giant.

<sup>3</sup>: Joint emission by both components of the Sz 108 system.

corresponding to the saturation limit for chromospherically active stars. Among the lowest mass members, most of the new H $\alpha$  emitters found by Comerón et al. (2003) are detected, including the M7.5 brown dwarf Par-Lup3-1. The emission levels of both Par-Lup3-1 and 3-3 are actually very close to the upper limits found by Comerón et al. (2003). Only an upper limit is available for Par-Lup3-4.

## 7. Individual Members

### 7.1. HR 5999 and HR 6000

The occurrence of Herbig Ae/Be stars in low-mass star forming regions is relatively common: HD 97048 in Chamaeleon I, R CrA and TY Cra in the Corona Australis cloud, and HD 147889 in the  $\rho$  Ophiuchi clouds are examples of this. The same is true for Lupus 3, whose visual appearance is dominated by the Herbig Ae/Be stars HR 5999 and HR 6000.

HR 5999 is one of the most extensively studied members of the Herbig Ae/Be class, a A5-7IVe+sh star lying on the pre-main sequence instability strip and illuminating a faint reflection nebula. Using its Hipparcos parallax (Table 1) and literature data, van den Ancker et al. (1998) derive a location near the stellar birthline (age  $0.6 \pm 0.4$  Myr), a temperature of 7600 K, a luminosity of  $78 L_{\odot}$ , and an extinction of  $A_V = 0.37$ . The extinction is found to be anomalous, possibly due to the depletion of small grains in the circumstellar envelope (Thé et al. 1996). In addition to an irregular variability of  $\Delta V = 0.35$  mag probably related to the circumstellar environment, it shows  $\delta$  Scuti-like pulsations with an amplitude of  $\Delta V = 0.013$  mag and a period of 4.99 h (Kurtz & Marang 1995), which can be accounted for by a model with a mass of  $4 M_{\odot}$  and a temperature of 7100 K (Marconi & Stahler 1998). HR 5999 is the first pre-main sequence star for which multiperiodic oscillations, including non-radial pulsations, have been detected (Kurtz & Catala 2001; Böhm et al. 2004). X-rays are detected in the direction of the star (Zinnecker & Preibisch 1994, Hünsch et al. 1998, Hamaguchi et al. 2005), but the emission may actually come from its possible T Tauri companion (Schröder & Schmitt 2007). It has a weak magnetic field (Hubrig et al. 2004). HR 5999 is a binary system with a visual secondary at  $1''.53$  (Ghez et al. 1997); see also Table 8. Note however that a slightly smaller separation,  $1''.45$ , is given by Stecklum et al. (1995). The primary shows in turn radial velocity variations that may be due to the presence of a close companion orbiting at 0.17 AU (Tjin A Djie et al. 1989), although the cause has not been confirmed thus far. The star displays strong mid-infrared excess with a broad silicate feature (Siebenmorgen et al. 2000). The disk emission around the primary has been observed by ISO and modeled by Acke & van den Ancker (2004), Acke et al. (2005), and Elia et al. (2004), and the ultraviolet spectrum of the star shows strong indications of variable accretion (Pérez et al. 1993).

HR 6000 is also a Herbig Ae/Be star (B6p; van den Ancker et al. 1996), hotter and probably at a somewhat later evolutionary stage than HR 5999. The star is a well-studied chemically peculiar star (Andersen et al. 1984) characterized by a strong underabundance of helium (Catanzaro et al. 2004 and references therein). Many other elements also show departures from solar abundances, being either above or below (Castelli et al. 1985), thus combining anomalies from a variety of Bp subtypes; see Castelli & Hubrig (2007). Strong X-ray emission is detected at its position (Zinnecker & Preibisch 1994), probably due to a T Tauri close companion rather than to the star itself. Photometric evidence for the companion, as well as a long-term, low-amplitude photometric variability, has been reported by van den Ancker et al. (1996), who also suggested that such a companion might be responsible for the misclassification of HR 6000 as a chemically peculiar star, a possibility that is virtually excluded by the analysis of Castelli & Hubrig (2007). Short-term variability with an amplitude of 0.004 mag and a period of 2.028 days has been observed by Kurtz & Marang (1995).

The rotation period can be made consistent with the very small rotational broadening of its spectral lines only by assuming an orientation very close to pole-on.

Like HR 5999, HR 6000 also shows mid-infrared excess emission, but the ISO spectrum presented by Siebenmorgen et al. (2000) shows it to be featureless and well reproduced by the Rayleigh-Jeans tail of a black body, in sharp contrast with the strong silicate feature of HR 5999.

## 7.2. RU Lup

The brightest member of Lupus 2, RU Lup, is one of the best studied classical T Tauri stars. A recent summary of its fundamental properties by Stempels & Piskunov (2002) yields  $T_{\text{eff}} = 3950$  K,  $\log g = 3.9$ ,  $L = 0.49 L_{\odot}$ ,  $R = 1.7 R_{\odot}$ ,  $M = 0.8 M_{\odot}$ , and  $v \sin i = 9$  km s<sup>-1</sup>. The low value of  $v \sin i$  suggests a nearly pole-on viewing geometry. A search for a magnetic field has set an upper limit of  $< 500$  G (Johnstone & Penston 1987). The rotation period is still somewhat controversial. A period of 0.8 days has been estimated by assuming that the inner edge of its accretion disk corotates with the star, in the extensive modeling of the accretion on the star carried out by Lamzin et al. (1996). Unfortunately, photometric monitoring (Giovannelli et al. 1991) does not yield a clear measurement of the rotation period, as the variability is highly irregular. However, radial velocity variations with a periodicity of 3.71 days have been recently measured by Stempels et al. (2007), which are attributed to spots on the surface of the star on the basis of a correlation between the slope of the absorption lines bisector and the radial velocity. This period is thus likely to represent the true rotation period of the star. Being both bright and a typical example of its class, RU Lup is currently receiving intense attention as a target for interferometry, most notably with the Very Large Telescope Interferometer.

Overall, the spectrum of RU Lup displays strong T Tauri features. The strong Balmer lines often show P Cygni profiles indicative of a high density outflow moving at a speed of  $\sim 100$  km s<sup>-1</sup> along the line of sight. Forbidden lines of [FeII], [SII], [OI] are formed in a lower density extended region (Lago 1982). No large-scale molecular outflow seems to be associated with the star, and the molecular gas in its surroundings is actually found to be rather quiescent (Gahm et al. 1993). The spectrum shows a high and variable degree of continuum veiling in the blue due to inhomogeneous accretion. A detailed view of short-scale variations in the accretion has been presented by Stempels & Piskunov (2002), who used the VLT to obtain a large number of high signal-to-noise spectra over a span of two nights. The shortest variability timescales are of order one hour, showing that they are not due to rotational modulation. The estimated accretion rate is  $3 \times 10^{-7} M_{\odot} \text{ yr}^{-1}$  (Lamzin et al. 1996), and up to  $10^{-6} M_{\odot} \text{ yr}^{-1}$  during flares. A more recent determination using Hubble Space Telescope far ultraviolet spectra gives  $5 \times 10^{-8} M_{\odot} \text{ yr}^{-1}$  (Herczeg et al. 2005). The profiles of the lines of highly ionized species of C, Si, and N testify to the complexity of the accretion process, as described in Lamzin et al.'s (1996) models. Further insight on the accretion process is provided by X-ray spectroscopy with XMM-Newton presented by Robrade & Schmitt (2007), where stable emission from dense plasma at  $2 - 3 \times 10^6$  K is detected and ascribed to the accretion shocks. The observations also show a distinct component of X-ray emission variable over timescales shorter than one month, produced by gas at higher temperatures ( $\simeq 30 \times 10^6$  K) probably related to coronal activity. Both components are also observed in other classical T Tauri stars.

The circumstellar disk is rather massive: observations of its emission at 1.3 mm by Nürnberger et al. (1997) yield a mass of  $2.3 \times 10^{-2} M_{\odot}$ , equivalent to more than 20 times the mass of Jupiter, or 2.8% of the mass of the central star when adopting Stempels & Piskunov's (2002) value cited above. The RU Lup disk is thus the second most massive in Lupus, slightly less massive than that of IM Lup (see Section 6.3.). However, it is not detected in CO by van Kempen et al. (2007), indicating that the gas associated with the disk is strongly depleted in that species.

The forbidden lines in the spectrum of RU Lup described by Stempels & Piskunov (2002), and particularly [OI], are asymmetric and characterized by the absence of a red tail in the line profile, whereas the blueshifted wing has a strong low velocity component and a high velocity component extending up to  $200 \text{ km s}^{-1}$ . Such two-component structure is common among T Tauri stars (e.g. Hartigan et al. 1995) and is normally interpreted as arising from the combination of a low-velocity wind and a high velocity collimated jet. Stempels & Piskunov (2002) find that the low-velocity component of the [OI] lines increases within hours of an accretion event, the latter being detected by an increase in veiling. The line asymmetry described above and the radial velocity of the high velocity component suggest a nearly pole-on viewing geometry, in which the redshifted component is blocked from view by the circumstellar disk. Similar profiles, as well as variability on timescales of hours and velocities of up to  $250 \text{ km s}^{-1}$ , are seen in the CaII H and K lines and the NaI D lines. The spatial structure has been studied in some detail by Takami et al. (2001) using the technique of spectroastrometry. With this technique the authors show that it is possible to discern details of emission-line regions on milliarcsecond scale. In their observations, the  $H\alpha$  emission appears displaced to either side of the star as a function of the velocity providing hints of the existence of a microjet, and the redshifted component is seen, probably through a gap in the disk whose width is estimated to be 3-4 AU. Further support for the existence of a wide gap, lying closer to the star, is provided by the near- and mid-infrared spectral energy distribution, which indicates a lack of dust at temperatures between 200 and 900 K, roughly corresponding to distances between 0.1 and 2 AU from the star. A close companion has been proposed as the possible cause of the gap, but searches with different techniques have failed to detect it (e.g. Bernacca et al. 1995, Ghez et al. 1997, Bailey 1997). Alternatively, Takami et al. (2001) speculate that a massive planet being formed around RU Lup may be the cause, which may also account for the fragmentary nature of the disk hinted at by near-infrared flux variations (Giovannelli et al. 1995).

Both the shape and position of the  $H\alpha$  emission region change over timescales of years. The [OI] and [SII] lines, with blueshifted components only, are observed only on one side of the star, the [OI] being closer to it as expected from higher critical density of [OI] with respect to that of [SII] (Hamann 1994). The width of other permitted lines, up to  $125 \text{ km s}^{-1}$ , is much lower than that of  $H\alpha$  (up to  $900 \text{ km s}^{-1}$ ; Reipurth et al. 1996). The long-term variability of the  $H\alpha$  line is modeled by Takami et al. (2001) as due to a steady outflow and a time-variable, unresolved inflow. More recently, Podio et al. (2008) have used near-infrared spectroscopy and spectroastrometry to investigate accretion and mass loss in RU Lup through Paschen and Brackett series lines of HI and the HeI line at  $1.083 \mu\text{m}$ . The P Cygni profile with broad blueshifted absorption detected in the HeI line is interpreted as evidence for a radial wind stemming directly from the star, rather than from the disk. At the same time, simple models of spherical accretion or winds cannot simultaneously explain the Paschen and Brackett decrements and line fluxes, suggesting a hybrid scenario in which line profiles and intensities are the result of non-spherical accretion and winds.

### 7.3. EX Lup

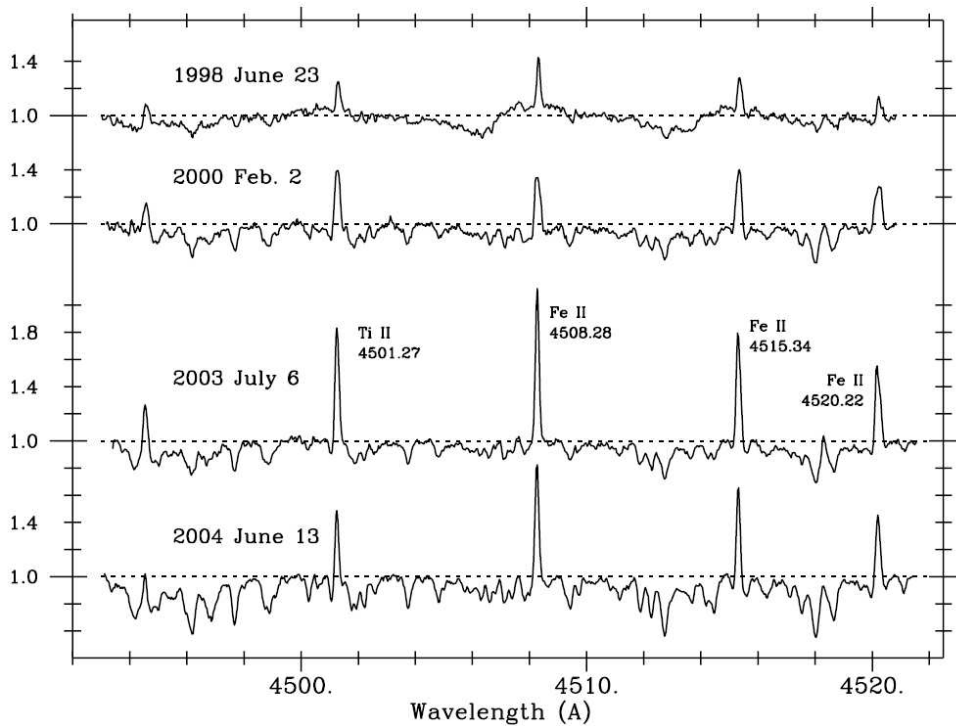


Figure 14. Sequence of spectra of EX Lup following an outburst, obtained with the HIRES spectrograph at the Keck telescope. Near the outburst peak (top spectrum) the narrow lines are superimposed on broad components with widths of a few hundred  $\text{km s}^{-1}$  displaying inverse P-Cygni profiles, with a redshifted absorption component at  $v \simeq +340 \text{ km s}^{-1}$  and a strong continuum veiling. As the outburst decays (second spectrum from the top) the broad components and redshifted absorption both disappear, and the veiling decreases. In the quiescent phase (two bottom spectra) the narrow lines and the photospheric absorption lines gain prominence due to the decrease of the veiling. The spectra are normalized to the continuum level. From Herbig (2007).

The apparently classical T Tauri star EX Lup was proposed by Herbig (1989) as the prototype of a new class of variables characterized by outbursts happening at irregular intervals, separated by periods of quiescence lasting for several years. The characteristics of the class are largely based on the individual characteristics of EX Lup itself, and have been summarized by Herbig (2007). The spectral type is late during the quiescent period (M0 in the case of EX Lup), during which the star displays a normal T Tauri emission line spectrum. During outbursts, which last from a few months to a few years, a broad component of the emission lines appears, accompanied by inverse P Cygni profiles with the absorption redshifted to  $> 300 \text{ km s}^{-1}$  from the narrow component. Simultaneously, the blue continuum veiling increases (see Fig. 14). The outbursts are interpreted as transient intense accretion episodes (Lehmann et al. 1995; Herbig et al. 2001).

Some of these characteristics are reminiscent of the FU Ori variables, although at a milder scale. EX Lup outbursts are more frequent, have lower jumps in brightness,

and the accompanying spectral changes are less dramatic (see e.g. Hartmann (1998) for a review of properties and their interpretation). Based on this it has been proposed that EX Lup variables represent an intermediate stage in an evolutionary sequence that goes from FU Ori outbursts at the end of the protostellar phase, characterized by strong accretion episodes in which the star can gain up to  $10^{-2} M_{\odot}$  over one century, to the more quiescent disk accretion stage in the classical T Tauri stars.

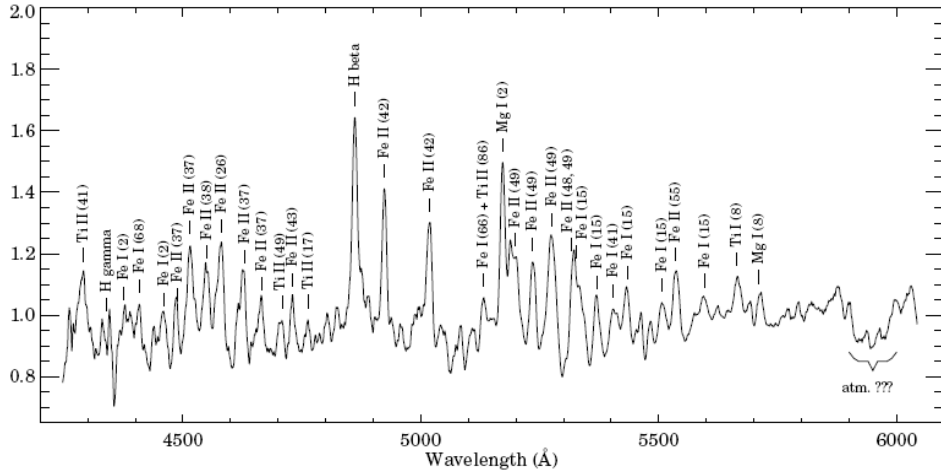


Figure 15. Spectrum of EX Lup at the peak of the extreme outburst of early 2008. This low-resolution spectrum is the average of 13 obtained in an interval of less than one month in January and February 2008. From Kóspál et al. (2008).

Few objects of the EX Lup class are known, and their actual membership in the class is uncertain (Herbig 2008). As pointed out by Herbig (2007), DR Tau, an object that was included in the original list of representatives of the class, differs in some of the defining characteristics from EX Lup, in the sense that the outburst duration is longer, the broad-line component is more prominent, and substantial variability persists during the quiescent phase. The differences among members of the class supports the interpretation of EX Lup stars as transition objects, in which the intensity of the accretion episodes greatly influences their observational features. Furthermore, even the defining characteristics of EX Lup itself are uncertain, as dramatically demonstrated by its latest outburst, started in January 2008 and still going on at the time of writing. In this outburst EX Lup has become brighter than ever in its recorded history, and its spectroscopic characteristics (see Figure 15) seem to differ markedly from those observed in previous outbursts (Kóspál et al 2008).

#### 7.4. HH 55

The HH 55 shock-excited nebula, initially reported by Schwartz (1977), lies near RU Lup, and earlier studies assumed a physical relationship between both. This was questioned by Cohen et al. (1986), who detected a M3.5 reflection spectrum clearly different from the K type of RU Lup. Reipurth & Wamsteker (1983) detected a near-infrared source embedded in HH 55, and Cohen & Schwartz (1987) resolved the IRAS source associated with RU Lup (Section 5.) into two components, one of them probably related to HH 55 and proposed as its driving source. Heyer & Graham (1990) found the

source to be faintly visible at  $R$ , and placed it near the main sequence on the basis of its position in the temperature-luminosity diagram. Further observations by Graham & Chen (1994) discovered an optical jet extending  $55''$  North and  $35''$  South of the central source, which appears elongated in images taken through both the  $H\alpha$  and the [SII] filters. These authors derive an age of 30 Myr based on theoretical evolutionary tracks. Their interpretation, tentatively applied also to Th 28 (see Section 7.5.) and other objects, assumes them to be aging jets produced by the central star at an age when accretion has stopped. Such interpretation is nevertheless challenged by the discovery of other objects sharing very similar properties and having luminosities that place them *below* the main sequence (e.g. Comerón et al. 2004, Fernández & Comerón 2005); see Sections 7.5. and 7.6.

### 7.5. Th 28

The remarkable object Th 28 is near the center of the Lupus 3 cloud, North of the HR 5999/6000 pair. It was initially identified as a T Tauri member of Lupus 3 by Thé (1962) and confirmed as an emission-line object by Schwartz (1977) and Appenzeller et al. (1983). However, its unusual character was noted by Krautter (1986), who discovered and studied its associated bipolar jet, HH 228 (see Section 5.). Further observations of the jet have been described by Graham & Heyer (1988) and by Coffey et al. (2004), who detected systematic radial velocity asymmetries along the jet that are interpreted as evidence for rotation at its base, where collimation and acceleration take place.

Th 28 is a very blue source with a very rich emission line spectrum superimposed on an unusually faint continuum (see e.g. Comerón et al. 2003). The spectral type of the central source is rather uncertain, but it has been estimated to lie in the G8-K2 range (Graham & Heyer 1988). The prominence of the emission lines is caused by the weakness of the underlying continuum: the  $H\alpha$  equivalent width reaches nearly  $400 \text{ \AA}$ , but the intrinsic luminosity of the line is not unusual for classical T Tauri stars. The accretion rate is estimated from ultraviolet lines to be between  $1.5 \times 10^{-7}$  and  $1.4 \times 10^{-6} M_{\odot} \text{ yr}^{-1}$  (Johns-Krull et al. 2000).

The faintness of the central source was already noted by Krautter (1986) and Hughes et al. (1994), who indicated as a preferred explanation an edge-on disk blocking most of the light from the central star. The central object would then be seen in scattered light, which would account for both its faintness and its unusually blue colors. Such explanation has been verified for other sources where direct imaging of the edge-on disk is feasible, most notably HH 30 (see e.g. Cotera et al. 2001), but to date not for Th 28 itself. Chapman et al. (2007) note that Spitzer measurements in the mid infrared do not display the double-peaked spectral energy distribution typical of nearly edge-on disks, and a direct imaging search for the hypothetical disk with the Hubble Space Telescope (Stapelfeldt et al., in preparation) has turned up negative results. Furthermore, despite the important role that a blocking disk plays in such scenario, the millimeter observations of Nürnberger et al. (1997) could set only an upper limit to the mass of the Th 28 disk of  $3.3 \times 10^{-3} M_{\odot}$ . The cause for the low luminosity of the central source of Th 28 thus remain unclear at the time of writing.

### 7.6. Par-Lup3-4

Par-Lup3-4 is a faint object in Lupus 3 whose strong emission-line spectrum was first reported by Comerón et al. (2003). Nakajima et al. (2000) had already identified it as



Figure 16. Narrow-band [SII] image obtained with FORS1 at the VLT centered on Par-Lup3-4, showing its small bipolar jet, HH 600. The image is  $70''$  in size, with North at the top and East to the left. The stripes near the top left of the image is due to internal reflections in the instrument caused by nearby bright stars.

a possible faint member of Lupus 3 in their near-infrared imaging survey. Comerón et al. (2003) measure a  $H\alpha$  equivalent width of approximately  $400 \text{ \AA}$  as well as the presence of numerous permitted and forbidden emission lines. The rich emission-line spectrum does not prevent a fairly accurate spectral classification, which is given as M5. Like in the case of HH 55, Th 28, and several other known examples, Par-Lup3-4 has an apparent age of  $\sim 50 \text{ Myr}$ , much older than that of other members of Lupus 3. Based on the prominence of some lines like HeI and the CaII infrared triplet, all of which are expected to form close to the surface of the object, Comerón et al. (2003) encounter difficulties in explaining the characteristics of the emission-line spectrum and of the photospheric continuum as an edge-on disk, and propose that the apparent underluminosity may be real and related to accretion on a very low mass object. This view has been however disputed by Barrado y Navascués et al. (2004b) for an object with characteristics very similar to those of Par-Lup3-4, LS-RCrA-1, for which an edge-on disk scenario is favored instead.

The recent discovery of a small faint jet, HH 600, extending from Par-Lup3-4 reported by Fernández & Comerón (2005) (Figure 16) shows that at least in the case of Par-Lup3-4 a certain degree of departure from edge-on is necessary to account for the double peak observed in the [SII] lines. Although the spatial velocity of the jet is unknown, a reasonable estimate based on typical jet speeds suggest an inclination greater than  $8^\circ$  from the plane of the sky, and even larger if jets of such late-type, low mass objects have velocities lower than those of their higher mass counterparts. Fernández & Comerón (2005) also find support for a non-edge-on geometry for LS-RCrA-1 based on forbidden line profiles, which hint at blocking of the red wing by a circumstellar disk. At this stage new observations at very high spatial resolution, as well as high resolution spectra of similar sources with high velocity outflows, seem to be the

most promising way of discerning on the actual cause for the strong underluminosity observed in this and other objects.

The mid-infrared spectral energy distribution of Par-Lup3-4, recently determined with Spitzer observations (Merín et al. 2007) is also unusual. Its infrared excess is moderate in the IRAC bands up to  $8 \mu\text{m}$ , but it increases dramatically in the  $24 \mu\text{m}$  MIPS band and goes on to become the 5th brightest source in Lupus 3 at  $70 \mu\text{m}$ , which may be indicative of the existence of an unusually large reservoir of cold dust around this object.

### 7.7. GQ Lup

GQ Lup is a classical T Tauri star in Lupus 1 with a K7-M0 spectrum. Hughes et al. (1994) derive an age near or below 2 Myr, and measure  $H\alpha$  emission with an equivalent width of  $38.4 \text{ \AA}$ . Other emission lines in its spectrum also have moderate strengths (Appenzeller & Wagner 1989). Its rotation period, determined from photometric variability probably due to hot spots, is found to be  $8.45 \pm 0.2$  days (Broeg et al. 2007), implying a viewing geometry  $27^\circ \pm 5^\circ$  away from pole-on. It has a substantial reservoir of circumstellar dust revealed by its mid-infrared properties (Weintraub 1990) and by its detection at 1.3 mm (Nürnberg et al. 1997). The latter measurements allow one to derive a circumstellar envelope mass of  $4.3 \times 10^{-3} M_\odot$ .

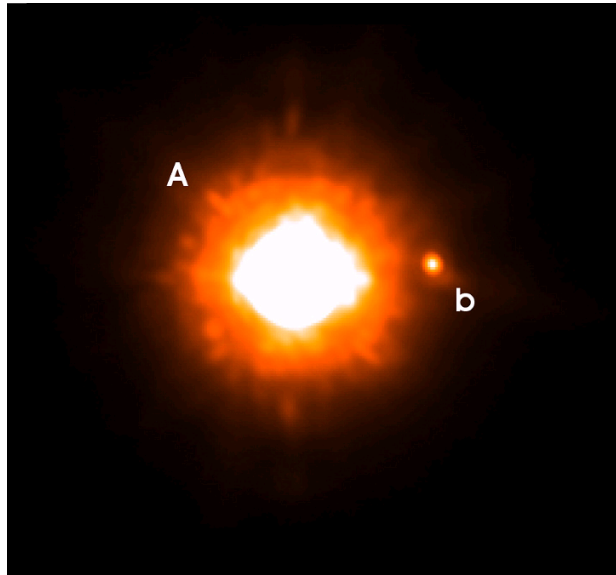


Figure 17.  $K_S$ -band image of GQ Lup and its very low mass companion obtained with the NACO adaptive optics camera at the Very Large Telescope. The separation is  $0''.73$ . North is up and East to the left.

While by all standards GQ Lup appears to be a normal classical T Tauri star, it has received much attention due to a recently discovered substellar companion, 6 mag fainter in the  $K$  band and lying  $0''.73$  from it (Neuhäuser et al. 2005), corresponding to a projected distance of 110 AU at an assumed distance of 160 pc for Lupus 1 (Figure 17). The physical relationship between both objects has been confirmed by astrometric measurements that show that both objects form a common proper motion pair,

with the possible detection of orbital motion consistent with an orbit close to edge-on (Neuhäuser et al. 2008). The faintness of the substellar companion together with its infrared colors suggest a late M or early L type, which was roughly confirmed by early spectroscopy and model fits that yielded a mass range between 1 and 42 Jupiter masses (Neuhäuser et al. 2005).

Later observations have made it possible to better constrain the physical parameters, which tend to place the companion of GQ Lup in the brown dwarf range domain rather than the planetary one. Marois et al. (2007) have used visible and near-infrared HST photometry to obtain a mass in the 10-20  $M_{\text{Jup}}$  range, and note an excess of flux in the red possibly caused by  $H\alpha$  emission, which suggests that the object may still be strongly accreting. These new results are supported by new integral field spectroscopy independently carried out by McElwain et al. (2007) and Seifahrt et al. (2007), which favor a somewhat earlier spectral type, in the M6-L0 range, and a mass between 10 and 40  $M_{\text{Jup}}$ . An independent upper mass limit of 35  $M_{\text{Jup}}$  has been proposed by Seifahrt et al. (2007) based on a comparison with the eclipsing double-lined brown dwarf binary 2M0535 (Stassun et al. 2006), whose components have a similar age. Despite the large uncertainties in the determination of the mass and other intrinsic parameters of the companion to GQ Lup, which are well summarized in Neuhäuser et al. (2008), the available results firmly place in the brown dwarf domain, most probably above the deuterium-burning limit but not excluding a mass as low as a few times that of Jupiter.

**Acknowledgments.** I am pleased to thank Belén López Martí for her careful reading of an earlier version of this article, as well as to Kengo Tachihara and Gabriel A.P. Franco for their useful input. I am also thankful to Bo Reipurth for his kind invitation to write this review and his numerous suggestions for improvement, and to a referee whose comments improved its readability. This review has made extensive use of the SIMBAD database, operated at CDS, Strasbourg, France, and of NASA's Astrophysics Data System.

## References

- Acke, B. & van den Ancker, M.E., 2004, *A&A*, 426, 151  
 Acke, B., van den Ancker, M.E. & Dullemond, C.P., 2005, *A&A*, 436, 209  
 Allen, P.R., Luhman, K.L., Myers, P.C., Megeath, S.T., Allen, L.E., Hartmann, L. & Fazio, G.G., 2007, *ApJ*, 655, 1095  
 Allers, K.N., Kessler-Silacci, J.E., Cieza, L.A. & Jaffe, D.T., 2006, *ApJ*, 644, 364  
 Alves, F.O. & Franco, G.A.P., 2006, *MNRAS*, 366, 238  
 Andersen, J. & Jaschek, M., 1984, *A&A*, 132, 354  
 André, P., Ward-Thompson, D. & Barsony, M., 1993, *ApJ*, 406, 122  
 Andreazza, C.M. & Vilas-Boas, J.W.S., 1996, *A&AS*, 116, 21  
 Appenzeller, I., Krautter, J. & Jankovics, I., 1983, *A&AS*, 53, 291  
 Appenzeller, I. & Wagner, S., 1989, *A&A*, 225, 432  
 Bailey, J., 1997, *MNRAS*, 301, 161  
 Baraffe, I., Chabrier, G., Allard, F. & Hauschildt, P.H., 1998, *A&A*, 337, 403  
 Baraffe, I., Chabrier, G., Allard, F. & Hauschildt, P.H., 2002, *A&A*, 382, 563  
 Barnard, E.E., 1927, *Catalogue of 349 dark objects in the sky*, Univ. of Chicago Press  
 Barrado y Navascués, D. & Jayawardhana, R., 2004a, *ApJ*, 615, 840  
 Barrado y Navascués, D., Mohanty, S. & Jayawardhana, R., 2004b, *ApJ*, 604, 284  
 Bernacca, P.R., Lattanzi, M.G., Porro, I., Neuhäuser, R. & Bucciarelli, E., 1995, *A&A*, 299, 933  
 Bertout, C., Robichon, N. & Arenou, F., 1999, *A&A*, 352, 574

- Blaauw, A., 1991, in *The Physics of Star Formation and Early Stellar Evolution*, NATO ASI Ser. C, 342, eds. C.J. Lada and N.D. Kylafis, p. 125
- Böhm, T., Catala, C., Balona, L. & Carter, B., 2004, *A&A*, 427, 907
- Breitschwerdt, D., Freyberg, M.J. & Egger, R., 2000, *A&A*, 361, 303
- Broeg, C., Schmidt, T.O.B., Guenther, E., Gaedke, A., Bedalov, A., Neuhäuser, R. & Walter, F.M., 2007, *A&A*, 468, 1039
- Cambrésy, L., 1999, *A&A*, 345, 965
- Cambrésy, L., Epchtein, N., Copet, E., de Batz, B., Kimeswenger, S., Le Bertre, T., Rouan, D. & Tiphène, D., 1997, *A&A*, 324, L5
- Castelli, F., 1985, *A&AS*, 59, 1
- Castelli, F. & Hubrig, S., 2007, *A&A*, 475, 1041
- Catanzaro, G., Leone, F. & Dall, T.H., 2004, *A&A*, 425, 641
- Chapman, N.L., Lai, S.-P. & Mundy, L.G., et al., 2007, *ApJ*, 667, 288
- Cieza, L., Padgett, D.L., Stapelfeldt, K.R., et al., 2007, *ApJ*, 667, 308
- Coffey, D., Bacciotti, F., Woitas, J., Ray, T.P. & Eisloffel, J., 2004, *ApJ*, 604, 758
- Cohen, M. & Schwartz, R.D., 1987, *ApJ*, 316, 311
- Cohen, M., Dopita, M.A. & Schwartz, R.D., 1986, *ApJ*, 307, L21
- Comerón, F., 1999, *A&A*, 351, 506
- Comerón, F., Torra, J. & Gómez, A.E., 1994, *A&A*, 286, 789
- Comerón, F., Neuhäuser, R. & Kaas, A.A., 2000, *A&A*, 359, 269
- Comerón, F., Fernández, M., Baraffe, I., Neuhäuser, R. & Kaas, A.A., 2003, *A&A*, 406, 1001
- Comerón, F., Reipurth, B., Henry, A. & Fernández, M., 2004, *A&A*, 417, 583
- Cotera, A., Whitney, B.A., Young, E., Wolff, M.J., Wood, K., Povich, M., Schneider, G., Rieke, M. & Thompson, R., 2001, *ApJ*, 553, 321
- Covino, E., Alcalá, J.M., Allain, S., Bouvier, J., Terranegra, L. & Krautter, J., 1997, *A&A*, 328, 187
- Cox, D.P. & Reynolds, R.J., 1987, *ARA&A*, 25, 303
- Crawford, I.A., 2000, *MNRAS*, 317, 996
- D'Antona, F. & Mazzitelli, I., 1994, *ApJS*, 90, 467
- de Geus, E.J., de Zeeuw, P.T. & Lub, J., 1989, *A&A*, 216, 44
- de Geus, E.J., 1992, *A&A*, 262, 258
- de Zeeuw, P.T., Hoogerwerf, R., de Bruijne, J.H.J., Brown, A.G.A. & Blaauw, A., 1999, *AJ*, 117, 354
- Dobashi, K., Uehara, H., Kandori, R., Sakurai, T., Kaiden, M., Umemoto, T. & Sato, F., 2005, *PASJ*, 57, S1
- Dubath, P., Reipurth, B. & Mayor, M., 1996, *A&A*, 308, 107
- Dullemond, C.P. & Dominik, C., 2005, *A&A*, 434, 971
- Elia, D., Strafela, F., Campeggio, L., Giannini, T., Lorenzetti, D., Nisini, B. & Pezzuto, S., 2004, *ApJ*, 601, 1000
- Esposito, M., Covino, E., Alcalá, J.M., Guenther, E.W. & Schisano, E., 2007, *MNRAS*, 376, 1805
- Evans, N.J., Allen, L.E., Blake, G.A., Boogert, A.C.A., Bourke, T., et al., 2003, *PASP*, 115, 965
- Feigelson, E.D., 1996, *ApJ*, 468, 306
- Fernández, M. & Comerón, F., 2005, *A&A*, 440, 1119
- Franco, G.A.P., 1990, *A&A*, 227, 499
- Franco, G.A.P., 2002, *MNRAS*, 331, 474
- Fuchs, B., Breitschwerdt, D., de Avillez, M.A., Dettbarn, C. & Flynn, C., 2006, *MNRAS*, 373, 993
- Gahm, G.F., Gebeyehu, M., Lindgren, M., Magnusson, P., Modigh, P. & Nordh, H.L., 1990, *A&A*, 228, 477
- Gahm, G.F., Johansson, L.E.B. & Liseau, R., 1993, *A&A*, 274, 415
- Ghez, A.M., McCarthy, D.W., Patience, J.L. & Beck, T.L., 1997, *ApJ*, 481, 378
- Giovannelli, F., Errico, L., Vittone, A.A. & Rossi, C., 1991, *A&AS*, 87, 89
- Giovannelli, F., Vittone, A.A., Rossi, C., Errico, L., Bisnovaty-Kogan, G.S., Kurt, V.G., Lamzin, S.A., Larionov, M., Sheffer, E.K. & Sidorenkov, V.N., 1995, *A&AS*, 114, 341

- Gondoin, P., 2006, *A&A*, 454, 595  
 Graham, J.A. & Chen, W.P., 1994, *AJ*, 108, 2273  
 Graham, J.A. & Heyer, M.H., 1988, *PASP*, 100, 1529  
 Greene, T.P., Wilking, B.A., André, P., Young, E.T., Lada, C.J., 1994, *ApJ*, 434, 614  
 Guillout, P., Sterzik, M.F., Schmitt, J.H.M.M., Motch, C. & Neuhäuser, R., 1998, *A&A*, 337, 113  
 Hamaguchi, K., Yamauchi, S. & Koyama, K., 2005, *ApJ*, 618, 360  
 Hamann, F., 1994, *ApJS*, 93, 485  
 Hara, A., Mizuno, A., Onishi, T., Kawamura, A., Obayashi, A. & Fukui, Y., 1999, *PASJ*, 51, 895  
 Hartigan, P., Edwards, S. & Ghandour, L., 1995, *ApJ*, 452, 736  
 Hartmann, L., 1998, *Astrophysical Processes in Star Formation* Cambridge Univ. Press  
 Henize, K.G., 1954, *ApJ*, 119, 459  
 Herbig, G.H., 1952, *JRASC*, 46, 222  
 Herbig, G.H., 1978, in *Problems of Physics and Evolution of the Universe*, ed. L.V. Mirzoyan, Publ. House of the Armenian Acad. of Sciences  
 Herbig, G.H., 1989, in *Proceedings of the ESO Workshop on Low Mass Star Formation and Pre-main Sequence Objects*, ed. B. Reipurth, p. 233  
 Herbig, G.H., 2007, *AJ*, 133, 2679  
 Herbig, G.H., 2008, *AJ*, 135, 637  
 Herbig, G.H., Aspin, C., Gilmore, A.C., Imhoff, C.L. & Jones, A.F., 2001, *PASP*, 113, 1547  
 Herczeg, G.J., Walter, F.M., Linsky, J.L., Gahm, G.F., Ardila, D.R., Brown, A., Johns-Krull, C.M., Simon, M. & Valenti, J.A., 2005, *AJ*, 129, 2777  
 Heyer, M.H. & Graham, J.A., 1989, *PASP*, 101, 816  
 Heyer, M.H. & Graham, J.A., 1990, *PASP*, 102, 117  
 Hubrig, S., Schoeller, M. & Yudin, R.V., 2004, *A&A*, 428, L1  
 Hughes, J., Hartigan, P. & Clampitt, L., 1993, *AJ*, 105, 571  
 Hughes, J., Hartigan, P., Krautter, J. & Kelemen, J., 1994, *AJ*, 108, 1071  
 Hünsch, M., Schmitt, J.H.M.M. & Voges, W., 1998, *A&AS*, 132, 155  
 Jayawardhana, R. & Ivanov, V.D., 2006, *ApJ*, 647, L167  
 Johns-Krull, C.M., Valenti, J.A. & Linsky, J.L., 2000, *ApJ*, 539, 815  
 Johnstone, R.M. & Penston, M.V., 1987, *MNRAS*, 227, 797  
 Joy, A.H., 1945, *ApJ*, 102, 168  
 Kawamura, A., Onishi, T., Yonekura, Y., Dobashi, K., Mizuno, A., Ogawa, H. & Fukui, Y., 1998, *ApJS*, 117, 387  
 Kirkpatrick, J.D., Reid, I.N., Liebert, J., Cutri, R.M., Nelson, B., Beichman, C.A., Dahn, C.C., Monet, D.G., Gizis, J.E. & Skrutskie, M.F., 1999, *ApJ*, 519, 802  
 Knude, J. & Høg, E., 1998, *A&A*, 338, 89  
 Knude, J. & Nielsen, A.S., 2001, *A&A*, 373, 714  
 Kóspál, Á., Németh, P., Ábrahám, P., Kun, M., Henden, A. & Jones, A.F., 2008, *IBVS* No. 5819  
 Krautter, J., 1986, *A&A*, 161, 195  
 Krautter, J., 1991, in *Low Mass Star Formation in Southern Molecular Clouds*, ed. B. Reipurth, ESO Scientific Report no. 11, p. 127  
 Krautter, J., Wichmann, R., Schmitt, J.H.M.M., Alcalá, J.M., Neuhäuser, R. & Terranegra, L., 1997, *A&AS*, 123, 329  
 Kurtz, D.W. & Marang, F., 1995, *MNRAS*, 276, 191  
 Kurtz, D.W. & Catala, C., 2001, *A&A*, 369, 981  
 Lada, C.J. & Wilking, B.A., 1984, *ApJ*, 287, 610  
 Lago, M.T.V.T., 1982, *MNRAS*, 198, 445  
 Lamzin, S.A., Bisnovatyi-Kogan, G.S., Errico, L., Giovannelli, F., Katysheva, N.A., Rossi, C. & Vittone, A.A., 1996, *A&A*, 306, 877  
 Leahy, D.A., Nousek, J. & Hamilton, A.J.S., 1991, *ApJ*, 374, 218  
 Lehmann, T., Reipurth, B. & Brandner, W., 1995, *A&A*, 300, L9  
 Lombardi, M., Lada, C.J. & Alves, J., 2008, *A&A*, 480, 785

- Lommen, D., Wright, C.M., Maddison, S.T., Jørgensen, J.K., Bourke, T.L., et al. 2007, *A&A*, 462, 211
- López Martí, B., 2003, PhD Thesis, Univ. of Valencia, Spain
- López Martí, B., Eisloffel, J. & Mundt, R., 2005, *A&A*, 440, 139
- Makarov, V.V., 2007, *ApJ*, 658, 480
- Marconi, M. & Palla, F., 1998, *ApJ*, 507, L141
- Marois, C., Macintosh, B. & Barman, T., 2007, *ApJ*, 654, L151
- McElwain, M.W., Metchev, S.A., Larkin, J.E., Barczys, M., Iserlohe, C., Krabbe, A., Quirrenbach, A., Weiss, J. & Wright, S.A., 2007, *ApJ*, 656, 505
- Merín, B., Augereau, J.-C., van Dishoeck, E.F., et al., 2007, *ApJ*, 661, 361
- Merín, B., Jørgensen, J., Spezzi, L., Alcalá, J.M., Evans, N.J., et al., 2008, *ApJ*, in press
- Merrill, P.W., 1941, *PASP*, 53, 342
- Moreira, M.C. & Yun, J.L., 2002, *A&A*, 381, 628
- Murphy, D.C., Cohen, R. & May, J., 1986, *A&A*, 167, 234
- Myers, P.C. & Goodman, A., 1991, *ApJ*, 373, 509
- Nakajima, Y., Tamura, M., Oasa, Y. & Nakajima, T., 2000, *AJ*, 119, 873
- Nakajima, Y., Nagata, T., Sato, S., Nagayama, T., Nagashima, C., Kato, D., Kurita, M., Kawai, T., Tamura, M., Nakaya, H. & Sugitani, K., 2003, *AJ*, 125, 1407
- Neuhäuser, R., Guenther, E.W., Wuchterl, G., Mugrauer, M., Bedalov, A. & Hauschildt, P.H., 2005, *A&A*, 435, L13
- Neuhäuser, R., Mugrauer, M., Seifahrt, A., Schmidt, T.O.B. & Vogt, N., 2008, *A&A*, 484, 281
- Nozawa, S., Mizuno, A., Teshima, Y., Ogawa, H. & Fukui, Y., 1991, *ApJS*, 77, 647
- Nürnberg, D., Chini, R. & Zinnecker, H., 1997, *A&A*, 324, 1036
- Padgett, D.L., Cieza, L., Stapelfeldt, K.R., et al., 2006, *ApJ*, 645, 1283
- Pérez, M.R., Grady, C.A. & Thé, P.S., 1993, *A&A*, 274, 381
- Podio, L., Garcia, P.J.V., Bacciotti, F., Antonucci, S., Nisini, B., Dougados, C. & Takami, M., 2008, *A&A*, 480, 421
- Pöppel, W.G.L., 1997, *Fund. Cosm. Phys.* 18, 1
- Preibisch, T. & Zinnecker, H., 1999, *AJ*, 117, 2381
- Preibisch, T., Brown, A.G.A., Bridges, T., Guenther, E. & Zinnecker, H., 2002, *AJ*, 124, 404
- Reipurth, B. & Wamsteker, W., 1983, *A&A*, 119, 14
- Reipurth, B., 2000, *A General Catalogue of Herbig-Haro Objects*, 2nd ed., Univ. of Colorado
- Reipurth, B. & Graham, J.A., 1988, *A&A*, 202, 219
- Reipurth, B. & Zinnecker, H., 1993, *A&A*, 278, 81
- Reipurth, B., Pedrosa, A. & Lago, M.T.V.T., 1996, *A&AS*, 120, 229
- Riegler, G.R., Agrawal, P.C. & Gull, S.F., 1980, *ApJ*, 235, L71
- Rizzo, J.R., Morras, R. & Arnal, E.M., 1998, *MNRAS*, 300, 497
- Robrade, J. & Schmitt, J.H.M.M., 2007, *A&A*, 473, 229
- Schröder, C. & Schmitt, J.H.M.M., 2007, *A&A*, 475, 677
- Schwartz, R.D., 1977, *ApJS*, 35, 161
- Seifahrt, A., Neuhäuser, R. & Hauschildt, P.H., 2007, *A&A*, 463, 309
- Shu, F.H., Adams, F.C. & Lizano, S., 1987, *ARA&A*, 25, 23
- Shirley, Y.L., Evans, N.J., Rawlings, J.M.C. & Gregersen, E.M., 2000, *ApJS*, 131, 249
- Siebenmorgen, R., Prusti, T., Natta, A. & Mueller, T.G., 2000, *A&A*, 361, 258
- Stassun, K.G., Mathieu, R.D. & Valenti, J.A., 2006, *Nature*, 440, 311
- Stecklum, B., Eckart, A., Henning, Th. & Löwe, M., 1995, *A&A*, 296, 463
- Stempels, H.C. & Piskunov, N., 2002, *A&A*, 391, 595
- Stempels, H.C., Gahm, G.F. & Petrov, P.P., 2007, *A&A*, 461, 253
- Sterzik, M.F. & Durisen, R.H., 1995, *A&A*, 304, L9
- Strassmeier, K.G., Rice, J.B., Ritter, A., Küker, M., Hussain, G.A.J., Hubrig, S. & Shobbrook, R., 2005, *A&A*, 440, 1105
- Tachihara, K., Dobashi, K., Mizuno, A., Ogawa, H. & Fukui, Y., 1996, *PASJ*, 48, 489
- Tachihara, K., Mizuno, A. & Fukui, Y., 2000, *ApJ*, 528, 817
- Tachihara, K., Toyoda, S., Onishi, T., Mizuno, A., Fukui, Y. & Neuhäuser, R., 2001, *PASJ*, 53, 1081

- Tachihara, K., Rengel, M., Nakajima, Y., Yamaguchi, N., André, P., Neuhäuser, R., Onishi, T., Fukui, Y. & Mizuno, A., 2007, *ApJ*, 659, 1382
- Takami, M., Bailey, J., Gledhill, T.M., Chrysostomou, A. & Hough, J.H., 2001, 323, 177
- Teixeira, P.S., Lada, C.J. & Alves, J.F., 2005, *ApJ*, 629, 276
- Thé, P.S., 1962, *Contrib. Bosscha Obs.*, 15
- Thé, P.S., Pérez, M.R., Voshchninnikov, N.V. & van den Ancker, M.E., 1996, *A&A*, 314, 233
- Thi, W.F., van Dishoeck, E.F., Blake, G.A., van Zadelhoff, G.J., Horn, J., et al., 2001, *ApJ*, 561, 1074
- Tjin A Djie, H.R.E., Thé, P.S., Andersen, J., Nordström, B., Finkenzeller, U. & Jankovics, I., 1989, *A&AS*, 78, 1
- van den Ancker, M.E., de Winter, D. & Thé, P.S., 1996, *A&A*, 313, 517
- van den Ancker, M.E., Thé, P.S., Tjin A Djie, H.R.E., Catala, C., de Winter, D. & Blondel, P.F.C., 1998, *A&A*, 324, L33
- van Kempen, T.A., van Dishoeck, E.F., Brinch, C. & Hogerheijde, M.R., 2007, *A&A*, 461, 983
- Vilas-Boas, J.W.S., Myers, P.C. & Fuller, G.A., 2000, *ApJ*, 532, 1038
- Vrba, F.J., Marraco, H.G. & Strom, S.E., 1992, *AAS*, 181, 7707 (abstract)
- Walker, M.F., 1956, *ApJS*, 2, 365
- Weintraub, D.A., 1990, *ApJS*, 74, 575
- Wichmann, R., Krautter, J., Schmitt, J.H.M.M., Neuhäuser, R., Alcalá, J.M., Zinnecker, H., Wagner, R.M., Mundt, R. & Sterzik, M.F., 1996, *A&A*, 312, 439
- Wichmann, R., Sterzik, M., Krautter, J., Metanomski, A. & Voges, W., 1997a, *A&A*, 326, 211
- Wichmann, R., Krautter, J., Covino, E., Alcalá, J.M., Neuhäuser, R. & Schmitt, J.H.M.M., 1997b, *A&A*, 320, 185
- Wichmann, R., Bastian, U., Krautter, J., Jankovics, I. & Rucinski, S., 1998, *MNRAS*, 301, L39
- Wichmann, R., Covino, E., Alcalá, J.M., Krautter, J., Allain, S. & Hauschildt, P.H., 1999, *MNRAS*, 307, 909
- Yonekura, Y., Dobashi, K., Mizuno, A., Ogawa, H. & Fukui, Y., 1997, *ApJS*, 110, 21
- Zinnecker, H. & Preibisch, T., 1994, *A&A*, 292, 152